https://doi.org/10.5194/egusphere-2025-4558
Preprint. Discussion started: 13 October 2025

Chlorophyll-a Variation Trends in Marginal Seas: Assessing the Impact of Global warming and Anthropogenic Activities Using Time Series Satellite Data (1998-2020)

Nan Yao[1], Xiaoyu Zhang[1,2*], Lei Bi[1], Shuchang Ma[1], Andrew B. Cundy[3], Haiyan Jin[4], Renyi Liu[1]

[1]School of Earth Sciences, Zhejiang University, Hangzhou, 310058, China
[2]Hainan Institute, Zhejiang University, Sanya, 572000, China
[3]GAU-Radioanalytical, School of Ocean and Earth Science, National Oceanography Centre (Southampton), University of Southampton, Southampton, UK, SO14 3ZH
[4]State Key Laboratory of Satellite Ocean Environment Dynamics, Second Institute of Oceanography, Ministry of Natural Resources, Baochubei Road 36, Hangzhou 310012, PR China

Correspondence to: X. Zhang (zhang_xiaoyu@zju.edu.cn)

Abstract. Global warming has been identified as the main cause of the decline of surface chlorophyll-a (Chl-a) concentrations in the oceans. Conversely, an increase in Chl-a concentration has been observed in a number of marginal seas over recent decades due to increasing anthropogenic input of key nutrients. However, with the intensification of global warming, its impact on Chl-a in coastal waters has been rarely studied, with the superimposed effects of human regulation of nutrients emissions. This study utilized time series of oceanic color satellite data from 1998 to 2020 to examine the spatio-temporal distribution of Chl-a in a range of marginal sea areas, and its relationship with environmental factors, particularly with sea surface temperature (SST), photosynthetically active radiation (PAR) and surface wind speed (SWS) are considered as well. The results suggested that the sea areas examined with varying mixing and water exchange characteristics and degrees of human influence have differing responses (in terms of their Chl-a trends) to increasing SST. Specifically, eutrophic closed seas with weak hydrodynamic exchange capacity, like the Bohai Sea, increasing SST did not apparent suppress Chl-a concentration, but instead continuous increase in Chl-a was observed in the central of the sea. In comparison, the open marginal seas examined show strong negative relationships between SST and Chl-a with distance offshore regardless of the degree of pressure from human activities, indicating that expected global warming effects driving reductions in Chl-a are extending to nearshore / marginal sea areas. This trend may be exacerbated due to stricter environment management policies imposed in recent years which have reduced anthropogenic nutrient inputs. Distinct from the above effect of global warming, PAR and SWS shape Chl-a in ways that are strongly modulated by geography and climate. PAR is the dominant positive control only in the Amazon estuary, where equatorial cloudiness and high turbidity create a light-limited regime, so any PAR increase directly stimulates phytoplankton. In mid-latitude open waters, PAR is secondary to SST: its seasonal rise is coupled to SST and therefore correlates negatively with Chl-a once thermal stratification reduces nutrient supply. SWS emerges as a key driver in the three open regimes (East China Sea >US East Coast> Amazon shelf), through injecting nutrient-rich cold deep water and

https://doi.org/10.5194/egusphere-2025-4558
Preprint. Discussion started: 13 October 2025

episodically raise Chl-a. Inside the two enclosed seas (Bohai, Gulf of Mexico), correlations with both PAR and SWS are weak ($|r| < 0.2$); Thus, PAR and SWS control Chl-a in a complex way, but both are more or less links to SST and nutrients input. This study highlights the complex interaction between primary production, SST, nutrient inputs and exchange, and environmental protection controls under the dual pressures of changes in human activity and coastal development, and global warming.

1 Introduction

Marine phytoplankton account for approximately half of the Earth's primary productivity and play a key role in ocean biogeochemical cycles and global climate processes (Field et al., 1998). As a biocarbon pump (BCP) marine phytoplankton accounts for about 26% of the global carbon sink(Dai et al., 2022; Friedlingstein et al., 2022; Jin et al., 2020; Letscher et al., 2023). Phytoplankton biomass is not only a key index for monitoring marine ecology and environment, but also provides an important basis for accurate estimation of oceanic primary productivity, carbon sinks, and food security.

Numerous studies have indicated that an observed decline of phytoplankton biomass over the past century in global oceans, can be attributed to increasing sea surface temperature (SST) due to global warming(Baker and Geider, 2021; Behrenfeld et al., 2016; Boyce et al., 2010a; IPCC, 2021). Since the beginning of the 20th century, a general rise in SST (specifically, an average temperature increase of 0.6 °C in the upper ocean) has led to the strengthening of water column stratification. This limits vertical nutrient exchange, resulting in reduced nutrient concentrations in upper waters, which in turn limits the growth of phytoplankton(Mizuta and Wikfors, 2020). It has been estimated that 80% of the observed decline in marine phytoplankton biomass from 1899 to 2008 is related to climate change, with the rate of Chl-a concentration reduction increasing with distance offshore (Boyce et al., 2010a). (Cai et al., 2022; Geng et al., 2024; Zhang et al., 2019). In the Pacific and Atlantic oceans in particular, during 1998-2007, waters with low Chl-a concentration (Chl-a ≤ 0.07 mg/m3) expanded at an annual rate of 0.8 % – 4.3 % , replacing about 800,000 square kilometres of water with high Chl-a concentration each year (Gregg et al., 2005; Gregg and Rousseaux, 2014). Additionally, as one of the most prominent sources of interannual natural variability in the Earth's climate system, global warming may alter the frequency and intensity of El Niño-Southern Oscillation (ENSO) events, thereby inducing extensive positive or negative sea surface temperature (SST) anomalies across the Pacific and beyond. This introduces additional complexity in deciphering the SST-Chl-a concentration relationship at regional and interannual scales(Cai et al., 2022; Hou et al., 2024).

In contrast, near-shore phytoplankton biomass shows a long-term increase, despite the global rise in SST, which is believed to be due to anthropogenic eutrophication (e.g., Kong et al., 2019; Lee et al., 2019; Marrari et al., 2016; Boyce et al., 2010; Jickells, 1998). Regional studies present conflicting conclusions regarding the relationship between SST and Chl-a in coastal waters, which may be due to a number of different regional oceanographic and anthropogenic effects. Coastal regions with upwelling, such as the South China Sea (Siemer et al., 2021) and Bay of Bengal (Chowdhury et al., 2021), exhibit a clear negative correlation between Chl-a and SST. Here, notwithstanding nutrient inputs from land, upwelling plays a crucial role

https://doi.org/10.5194/egusphere-2025-4558
Preprint. Discussion started: 13 October 2025

in transporting colder deeper water with abundant nutrients to the sea surface, stimulating local phytoplankton population and resulting in the negative correlation between SST and Chl-a (e..g., Favareto et al., 2023; Chen et al., 2021). In other areas, nutrient run-off and other anthropogenic activities have generated strong increases in primary productivity from the mid-20th century, despite SST increases. For example in the Baltic Sea, an increase in cultural eutrophication since the 1950s has produced marked sedimentary changes in a range of organic geochemical indicators, including those reflecting increased phytoplankton biomass, that have been suggested as forming important secondary markers for the proposed Anthropocene epoch at this candidate Global boundary Stratotype Section and Point site (Kaiser et al., 2023). Other anthropogenically-enhanced processes were indicated to have changed the correlation between Chl-a and SST profoundly, include the impact of predation, especially in aquaculture areas, which can reduce phytoplankton biomass(e.g., Frau et al., 2021; Mao et al., 2020), and commercial fishing practices, which indirectly influence phytoplankton biomass by affecting the abundance of zooplankton and fish(Campos-Silva et al., 2021; Reid et al., 2000).

Besides, the complex effects of other physical factors such as photosynthetically active radiation (PAR) and surface wind speed (SWS) make it more difficult to clarify the impact on Chl-a in the upper layers from global warming. Photophysiological processes-namely photoinhibition under supersaturating irradiance and photoadaptation through adjustments in pigment composition, light-harvesting complex abundance, and non-photochemical quenching capacity, exert first-order control on upper-ocean Chl-a inventories(Moradi and Moradi, 2020; Pi et al., 2019). However, despite large previous efforts there are still significant gaps in the current understanding of the variability of Chl-a and its relation to the PAR on regional seasonal time scales. The influence of SWS on Chl-a is non-linear and spatially heterogeneous. Generally, moderate SWS intensifies coastal upwelling, injecting nutrient-rich deep water into the euphotic zone and stimulating phytoplankton growth. Whereas excessive wind forcing deepens the mixed layer and shortens residence time, impeding phytoplankton retention in the illuminated layer and ultimately suppressing biomass accumulation. Moreover, the magnitude and even the sign of this relationship vary with regional circulation and seasonal stratification(Wang and Xiu, 2022).

To better understand the controls on temporal and spatial Chl-a concentration trends in coastal waters, this study assesses the relationship between Chl-a concentrations (a proxy for phytoplankton biomass) and SST in five coastal waters with varying levels of anthropogenic activity, using time series satellite data from 1998 to 2020. Indices including PAR and SWS are also incorporated to comprehensively explore the underlying mechanisms driving the evolution of Chl-a. Specifically, we examine two enclosed bays with high levels of human interference (the Gulf of Mexico in the United States and Bohai Sea in China), and three open sea areas with varying degrees of human interference (the Amazon Estuary in Brazil, Eastern Coastal Waters of the US, and the Changjiang Estuary in the East China Sea of China). The objective is to elucidate the distinct responses of phytoplankton to sustained global warming in the presence of anthropogenic nutrient inputs and to distinguish the ecological effects of warming water intrusion from those of human activities.

The remainder of this paper is structured as follows. Data and Methods describes the study areas, satellite data sources, and the methodologies employed, including trend analysis, stability assessment, and correlation analysis. Results presents the spatiotemporal distribution characteristics of Chl-a, its historical variation trends, stability, and its relationship with key

https://doi.org/10.5194/egusphere-2025-4558
Preprint. Discussion started: 13 October 2025

environmental factors across the five marginal seas. Based on these findings, Discussion provides a comprehensive analysis of the mechanisms driving Chl-a variations, focusing on the roles of natural environmental factors, global warming, and anthropogenic nutrient inputs. Finally, Conclusions summarizes the main findings of the study and discusses their ecological implications under the dual pressures of global warming and human activity.

2 Data and Methods

2.1 Study areas

This study focuses on 5 Marginal Seas over the world with different water exchange rate and anthropogenic activities (shown in Fig. 1) (Cui et al., 2021; Lloyd et al., 2019; Dobson et al., 2000). The enclosed seas (here, Bohai Sea and Gulf of Mexico) are usually characterized by very slow water exchange, which limits the diffusion and transportation of land sourced pollutants and produces a limited self-purification capability. The three open sea areas studied were the Changjiang Estuary of East China Sea, the Eastern Coastal Waters of the US and Amazon Estuary. An open sea area is defined in this study relative to the enclosed sea area, that is, a near shore area with only one land boundary. Generally, the hydrodynamic conditions in open sea areas are favourable for the diffusion of land-derived materials.

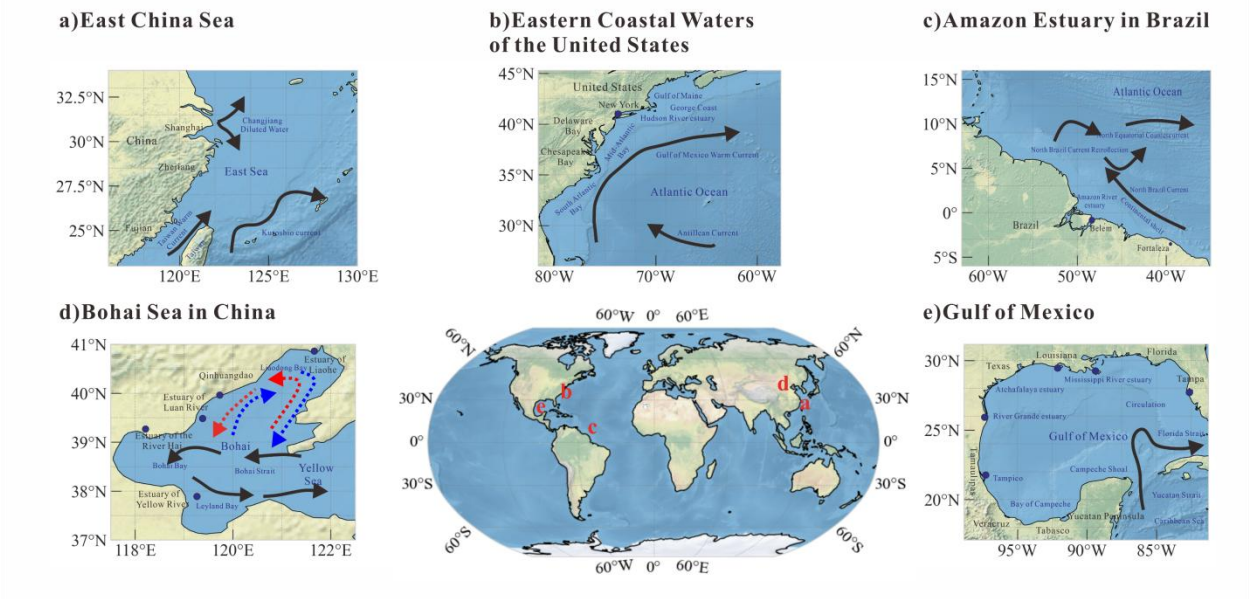

Figure 1. The geographical locations and major current systems of the five studied sea areas. a) East China Sea located in the range of 117 °E~131 °E and 23 °N~33°N; b) Eastern Coastal Waters of the US located in the range of 81.6°W – 57.66° W and 27.5°N – 43.3°N; c) Amazon Estuary located in the range of 16°N – 6°S and 61°W – 37°W; d) Bohai Sea located in the range of 37° N– 41°N and 117° E– 123°E; e) Gulf of Mexico located in the range of 17.09°N – 31.16°N and 98.86°W – 81.28°W. Note: The base maps for the land and ocean portions of the map artifacts are land cover data, and the ocean polygon data (rendered in grey), and are available for download from Natural Earth (https://www.naturalearthdata.com/).

https://doi.org/10.5194/egusphere-2025-4558
Preprint. Discussion started: 13 October 2025

The East China Sea is one of the biggest marginal seas of the northwestern Pacific with complex circulation systems (Fig. 1a). The Tsushima and Kuroshio currents with high temperature and salinity prevail in the eastern side of the East China Sea. On the western side, the Zhemin Coastal Currents, formed by the Changjiang River Plume (CRP) with the intrusion of the Taiwan Warm Current (TWC), dominate. However, due to increasing human activities in the Changjiang River Basin, there has been a significant increase in nutrient inputs, leading to more frequent occurrences of harmful algal blooms (HABs) (Zhou et al., 2022; Ministry of Ecology and Environment, PRC, 2001, 2021).

Eastern Coastal Waters of the US, located to the northeast of Gulf of Mexico, are strongly influenced by the Gulf Stream, resulting in enhanced primary productivity(Ma and Smith, 2022). Numerous rivers including the Hudson River, Delaware River, Susquehanna River, Joptank River, and others, flowing through highly urbanized cities, discharge pollutants and stimulated the frequency of HABs events increase in the past decades (e.g., Mizuta & Wikfors, 2020).

In Amazon Estuary in Brazil, the tropical Atlantic surface circulation, specifically the North Brazil Current running northwestward along the Brazilian coastline, exerts a dominant influence over the area (Fig. 1c). The Guyana Current is also active in this sea area. HABs in the Amazon Estuary typically occur during the spring and summer, as they are influenced by the seasonal flow variations of the Amazon River. Notably, there has been an increase in HAB events since 2008 (e.g.,Dai et al., 2023; Hallegraeff et al., 2021; Subramaniam et al., 2008).

The Bohai Sea is undergoing severe anthropogenic disturbance with coastal runoff from at least 40 rivers, such as the Yellow River, Haihe River, Liaohe River, and so on. The influx of significant amounts of pollutants, including sewage, has severely disrupted the local aquatic ecology (Ministry of Ecology and Environment, PRC, 2021). The circulation of the Bohai Sea exhibits seasonal variations (Fig. 1 d), significantly impacting the transport of pollutants. The rate of seawater exchange with the Yellow Sea strongly influences the ecological environment within the Bohai Sea (Ju et al., 2020).

The circulation system in the southeast of the Gulf of Mexico (Fig. 1f) act as the primary hydrodynamic force, stimulating the local primary productivity (Damien et al., 2021). Whereas, the northern part of the Gulf of Mexico is significantly influenced by nutrient inputs originating from the Mississippi-Atchafalaya Basin. The accelerated growth of industry and extensive use of fertilizers have led to excessive production of algae (e.g., Fu et al., 2020; Yingling et al., 2022) .

Table 1. Comparative environmental and demographic overview of study regions

Sea area	Attribute of the sea area	Hydrodynamic exchange capability	Population density of the basin (population/km²)	Eutrophic state	Human regulation
East China Sea	Open	High	563.88	High	Very High
Eastern Coastal	Open	High	151.28	Moderate to High	High

https://doi.org/10.5194/egusphere-2025-4558
Preprint. Discussion started: 13 October 2025

Waters of the US					
Amazon Estuary	Open	High	36.91	Low	Low
Bohai Sea	Enclosed	Moderate	344.78	High	Very High
Gulf of Mexico	Enclosed	High	71.61	Moderate to High	High

The five selected sea areas cover varying degrees of human activity and hydrodynamic exchange capability, as summarized in Table 1. Population density data for the surrounding basins (Table 1) were obtained from the LandScan (2020) high-resolution global population dataset (Lebakula et al., 2025) and are used here as a proxy for anthropogenic pressure. The term "Human regulation" in this context quantifies the intensity of human activities within the basin that regulate nutrient inputs and environmental stress on the marine ecosystem.

2.2 Data Sources

Concerning the influence by various chemical, hydrological, meteorological and biological factors (e.g., Hong et al., 2023; Xi et al., 2021; Martinez et al., 2020), the satellite derived datasets of Chl-a, combined with SST, PAR and SWS, are used to discuss temporal and spatial variation trends and interactions. Meanwhile, SST are also used to identify periods of which the seawater was heated. PAR and SWS were included as key environmental indices known to influence phytoplankton growth and distribution. PAR directly constrains photosynthesis, while SWS affects vertical mixing, nutrient entrainment from deeper layers, and light availability by modulating the mixed layer depth. Tab. 2 shows data types, data sources, temporal and spatial resolution, spanning periods and download websites used in this study.

Data type	Data sources	Temporal/spatial resolution	Periods	Links
Chl-a	SeaWiFS L3 Product	Monthly/9.28 km	1998.1~2010.12	https://oceancolor.gsfc.nasa.gov/l3/order/
	Aqua-MODIS L3 Product	Monthly/4.64 km	2008.1~2020.12	https://oceancolor.gsfc.nasa.gov/l3/order/
PAR	SeaWiFS L3 Product	Monthly/9.28 km	1998.1~2010.12	https://oceancolor.gsfc.nasa.gov/l3/order/

https://doi.org/10.5194/egusphere-2025-4558
Preprint. Discussion started: 13 October 2025

	Aqua-MODIS L3 Product	Monthly/4.64 km	2008.1~2020.12	https://oceancolor.gsfc.nasa.gov/l3/order/
SST	AVHRR Pathfinder SST	Monthly/0.25 deg	1998.1~2020.12	https://www.ncei.noaa.gov/products/avhrr-pathfinder-sst
SWS	CCMP Wind Vector Analysis Product	Monthly/0.25 deg	1998.1~2020.12	https://www.remss.com/measurements/ccmp/
Ocean boundary	Natural Earth Ocean	-/110m	-	https://www.naturalearthdata.com/downloads/110m-physical-vectors/110m-ocean/

Table 2. Monthly satellite derived datasets used in this study

These datasets, derived through algorithmic processing of raw satellite imagery, are recognized for their reliability and comprehensive temporal coverage, making them particularly valuable for studying waters with complex optical properties, such as coastal and estuarine environments. (Pisano et al., 2016; Zhang et al., 2006). We utilized an applicable method to establish the satellite dataset for those from different satellites, such as Chl-a and PAR: before constructing the time series dataset, however, the satellite Chl-a and PAR data were divided into three periods according to availability of different satellite products. (T1 period: Jan 1998-Dec 2002, Chl-a and PAR products only from SeaWiFS are available; T2 period: Jan 2003-Dec 2010, overlap period, Chl-a and PAR products from both MODIS and SeaWiFS are available; T3 period: Jan 2011-Dec 2020, Chl-a and PAR products are available only from MODIS) The two types of data products have different coverage times, so systematic errors is eliminated before merging them into a long-term data set. See Appendix A for an in-depth explanation of the data preprocessing methodology. The SST data, critical for the study, were extracted from the AVHRR Pathfinder dataset (Pisano et al., 2016). Additionally, SWS data were incorporated from the CCMP Wind Vector Analysis Product (Mears et al., 2019).

2.3 Methods

Fig. 2 shows a flowchart of this study. Based on the construction of satellite datasets of Chl-a, PAR, SWS and SST (from 1998 to 2020), the correlation and interaction between Chl-a changes and seawater warming was sorted out following the steps below: (1) the temporal trends of seasonal and annual Chl-a in the five different study areas were analyzed using the Mann-Kendall (M-K) Trend Analysis method. (2) the Chl-a stability and variation coefficients of each pixel were calculated to evaluate the varying degree of Chl-a spatially, and correlation analyses and PCA (principal component analyses) were conducted to determine the main marine environmental factors impacting Chl-a in each sea area. (3) the global warming

https://doi.org/10.5194/egusphere-2025-4558
Preprint. Discussion started: 13 October 2025

periods are identified with SST dataset. (4) image-by-image metric correlations between Chl-a and anthropogenic SST rising were calculated for specific time periods of interest.

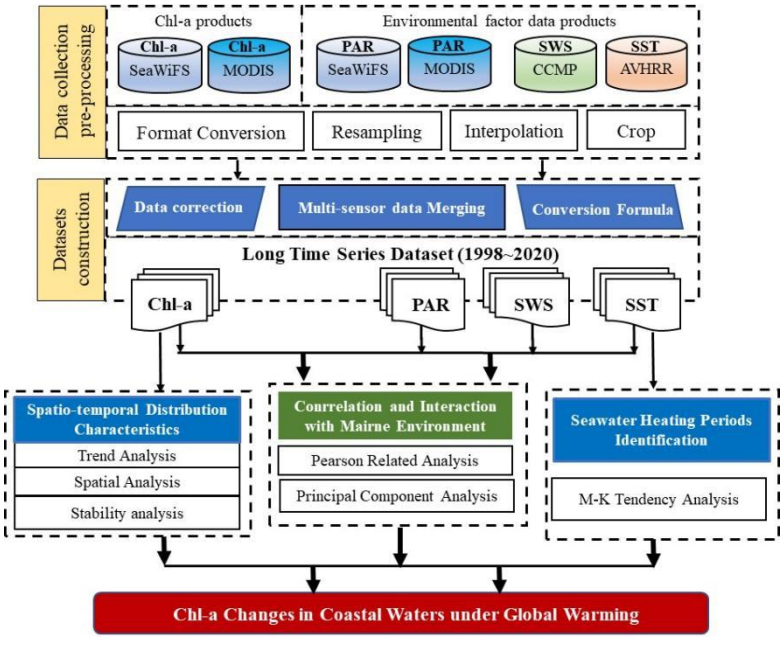

Figure 2. Flowchart for assessing the impact of global warming and anthropogenic activities on Chl-a trends using time-series satellite data

2.3.1 Time Series Analysis

The least squares method, widely used in time series analyses related to climate change (Mudelsee, 2019), was applied to obtain trends in Chl-a concentration over the period 1998-2020. The time series for trend analysis was composed of Chl-a values for each pixel in the study area, with outliers removed if they exceeded three times the standard deviation from the mean. See Appendix B for details of calculation. The results obtained are used to assess the local Chl-a response to global warming.

The M-K Trend Analysis method is a non-parametric statistical approach widely employed to discern temporal trends in time series data(e.g., Wang et al., 2021). This method assesses whether there is a statistically significant increasing or decreasing trend by comparing the relative ranks of data points over time. The test statistic UF (Upward Factor) is calculated to identify the sequence of potential upward trends, while UB (Downward Factor) is derived from the reversed data series to pinpoint the timing of potential trend shifts. The formulas for UF and UB are as follows:

$$UF_k = \frac{s_k - E(s_k)}{\sqrt{Var(s_k)}}, (k = 1,2,\dots,n) \quad (2\text{-}4)$$

https://doi.org/10.5194/egusphere-2025-4558
Preprint. Discussion started: 13 October 2025

$$UB_k = \frac{E(s_k) - s_k}{\sqrt{Var(s_k)}}, (k = 1,2,\dots,n) \quad (2\text{-}5)$$

of which s_k is a statistical measure defined in the Mann-Kendall test; $Var(s_k)$ represents the variance of the calculated statistical measure; $E(s_k)$ represents the expected value of the statistical measure. The relevant calculation formulas can be referred to Appendix C.

In the M-K test, the null hypothesis of no trend is rejected at the 5% significance level if the absolute value of UF exceeds 1.96. A positive UF value indicates an upward trend, while a negative value indicates a downward trend. The intersection point of the UF and UB curves, if it occurs within the confidence limits, suggests the year of a potential abrupt change in the trend. The detailed discrimination criteria for trend significance and direction are summarized in Tab.3.

Table 3. Discrimination criteria for M-K test

Threshold	$\alpha < 0.05(-1.96 \le UF \le 1.96)$	$\alpha \ge 0.05(UF > 1.96 \parallel UF < -1.96)$
$UF > 0$	Increasing but not significant	Significant increasing
$UF < 0$	Decreasing but not significant	Significant decreasing

where α is the level of confidence.

2.3.2 Spatio-temporal trends analysis

The slope analysis method (Wang, 2006) was employed to analyse the spatio-temporal trends of Chl-a in different five locations. From 1998 to 2020, the annual variation rate of Chl-a was calculated with the least squares method using time-series data from each pixel within the study region. A slope>0 indicates an upward trend of Chl-a at the corresponding pixel, and vice versa. The larger the value, the faster the increase, see Appendix C for details.

The stability of Chl-a is calculated by computing the Coefficient of Variation (CV) of Chl-a time-series data for each pixel, Chl-a stability is classified into five levels based on CV values: "High Stability" (CV < 0.05) indicates minimal variability; "Medium to High Stability" (0.05 ≤ CV < 0.10) reflects minor fluctuations; "Medium Stability" (0.10 ≤ CV < 0.15) shows moderate variability; "Medium to Low Stability" (0.15 ≤ CV < 0.20) represents significant fluctuations; and "Low Stability" (CV ≥ 0.20) signifies highly unstable conditions, see Appendix D for details.

2.3.3 Seawater Heating Period Identification

The warming periods were identified based on SST changes during 1998-2020 in the five locations using a four-year moving time window (Fig. 3). This window length was chosen to capture sustained, low-frequency warming signals indicative of climate-scale changes, while smoothing out shorter-term interannual variability (e.g., linked to seasonal cycles or transient weather events). Periods exhibiting the most pronounced SST rise within these 4-year windows were selected for analyzing

https://doi.org/10.5194/egusphere-2025-4558
Preprint. Discussion started: 13 October 2025

the interaction between Chl-a and SST increase. For comparison, periods of relatively stable SST were identified using the same 4-year window methodology.

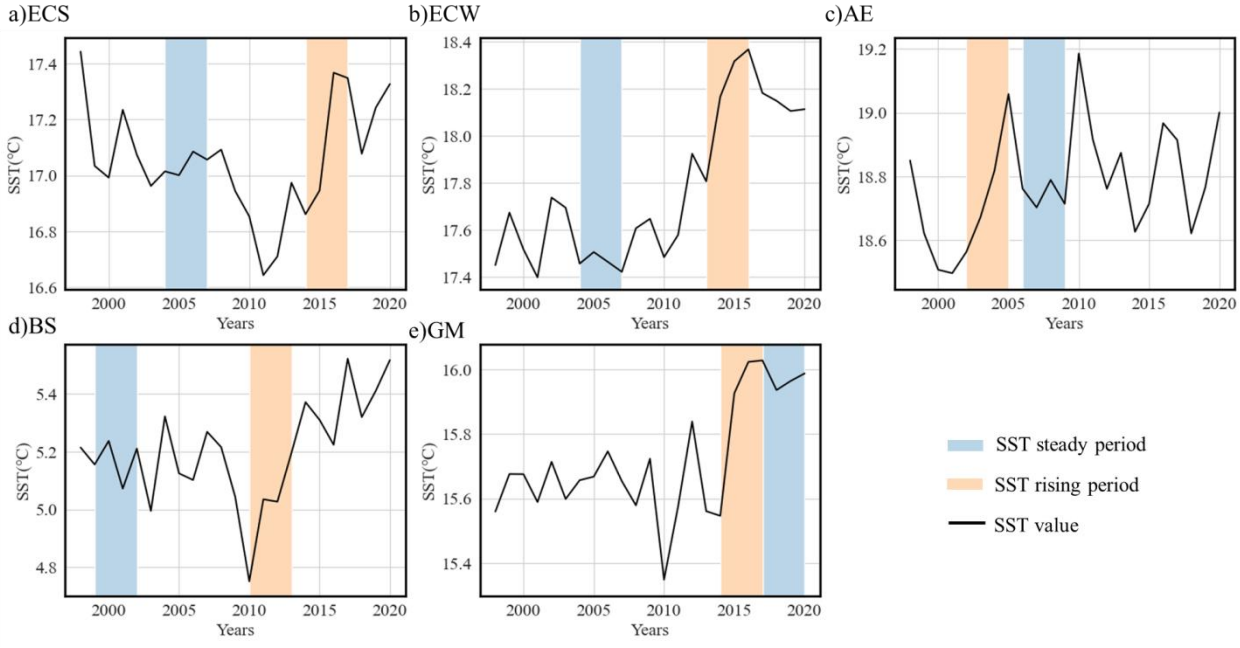

Figure 3. The variation of SST of the five locations from 1998 to 2020, and identified periods of SST rise and periods of SST stability.

Two time windows identified with the largest SST rise and the most stable SST in the five locations are shown in Tab. 4. The largest SST rising periods exhibit significant variation rates, reaching up to 0.120–0.200℃/yr. In contrast, the most stable SST periods correspond to variations of approximately 0.005–0.010℃/yr. The main SST rising periods of GM, ECS, and ECW tally with the time windows of the most intense El Niño event recorded (2014-2016), whereas distinct rises in SST for AE and BS are coincident with the occurrence of the El Niño windows of 2002-2003 and 2009-2010, respectively(Cai et al., 2021).

Table 4. Periods identified with different SST variation trend

Sea area type	Sea area	SST steady period	SST rising period		
			Period	SST rising(℃)	SST rising rate(℃/yr)
Open sea area	ECS	2004~2007	2014~2017	0.488	0.189
	ECW	2004~2007	2013~2016	0.561	0.183
Enclosed sea area	AE	2006~2009	2002~2005	0.495	0.163
	BS	1999~2002	2010~2013	0.445	0.133

https://doi.org/10.5194/egusphere-2025-4558
Preprint. Discussion started: 13 October 2025

GM	2017~2020	2014~2017	0.482	0.154

2.3.4 Correlation Analysis

We performed Pearson correlation and PCA to identify the impacts on the Chl-a concentrations from environmental factors for each study area. Specially(Maćkiewicz and Ratajczak, 1993), to understand how global warming affects phytoplankton in coastal sea waters, quantitative determination of the correlation between Chl-a concentrations and SST for each pixel within the study area are performed in SST stable period and in SST rising period respectively. In detail, the time series data for annual mean Chl-a and SST were normalized to address their inherent non-normal distribution. Through comparing the changes in correlations between Chl-a and SST across different sites, under conditions of thermal variation and stability, and considering the local hydrological characteristics, we delve into the mechanisms by which global warming influences Chl-a.

3 Results

3.1 Spatial distribution characteristics of Chl-a

Fig. 4 shows the seasonal and annual spatial distribution of Chl-a concentrations for the five study areas. All locations show distinct decreasing Chl-a with distance offshore, and higher values are mainly found in estuaries and bays. Particularly, areas with higher Chl-a are more uniformly distributed in the closed sea areas, particularly in the Bohai Sea, while Gulf of Mexico show similar spatial distribution tendency to those open sea areas.

From highest to lowest, Chl-a concentration varies in the order Bohai Sea > East China Sea> Gulf of Mexico> Eastern Coastal Waters of the US≈Amazon Estuary. As a severely eutrophic enclosed sea are, Bohai Sea maintains high values between 1.6 and 2.5 mg/m^3 throughout the year. Meanwhile the East China Sea, which is an open sea in highly eutrophic state, shows a consistently higher annual Chl-a, and Chl-a higher than 0.6 mg/m^3 in spring is frequently observed. The rest three regions all have year-round Chl-a below 0.6 mg/m^3.

Chl-a concentrations in the open sea area exhibit greater susceptibility to seasonal variations than those in enclosed seas as show in Fig. 4f, with change of the monthly average rate of Chl-a concentration surpassing 50%. This is in stark contrast to the Bohai Sea and the Gulf of Mexico, where the change rates of monthly variation are 18.97% and 16.32% respectively, neither exceeding the 20%.

https://doi.org/10.5194/egusphere-2025-4558
Preprint. Discussion started: 13 October 2025

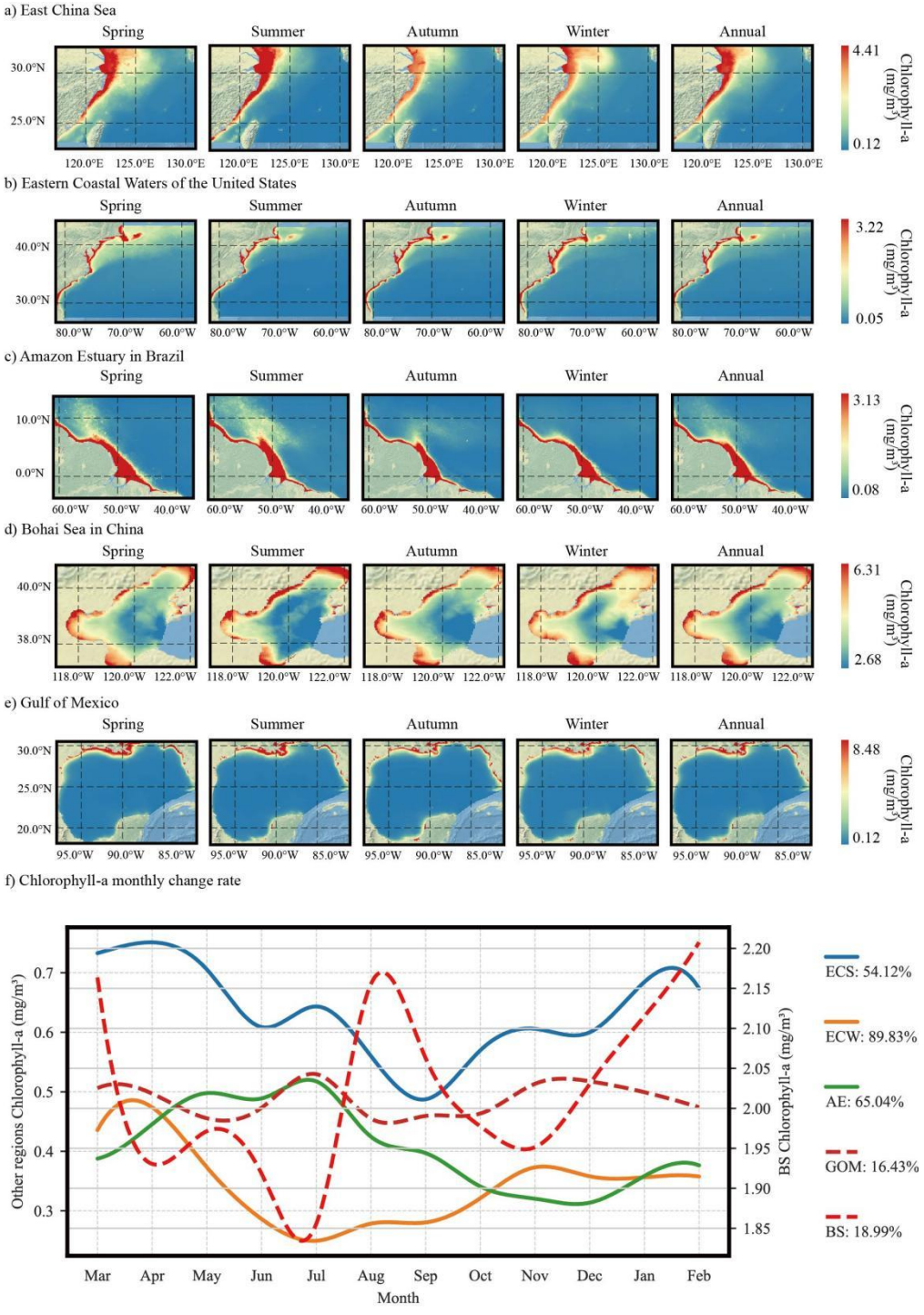

Figure 4. Spatial distribution of annual and seasonal Chl-a at the five sites. (a)- (e) represents East China Sea, Eastern Coastal Waters of the United States, Amazon Estuary, Bohai Sea, and Gulf of Mexico respectively. f presents the monthly variation of Chl-a concentrations in these regions. The Bohai Sea utilizes the right y-axis, while the other four

https://doi.org/10.5194/egusphere-2025-4558
Preprint. Discussion started: 13 October 2025

seas use the left y-axis. The data in the right is the monthly change rate. Areas shown in light grey blue (■) have no available data.

3.2 Historical Chl-a variation in study regions

With MK trend test, Chl-a concentration exhibits different temporal change tendency among the five locations (Fig. 5). Specially, a statistically significant overall increasing trend is suggested in annual and all seasonal Chl-a concentrations in the Gulf of Mexico ($p < 0.05$). While slight increase tendency of Chl-a is observed in the Eastern Coastal Waters of the US with a rate of 0.0301 $mg/m^3 \cdot a$, no statistically significant trends ($p > 0.05$) are observed in the East China Sea, U.S. East Coast, Amazon Estuary, or Bohai Sea. However, distinct continuous increase of Chl-a is indicated in summer in sea area of U.S. East Coast.

Notably, both Bohai Sea and the East China Sea exhibit a two-stage change, with decreasing tendency after a continuous increasing, although the decline of the East China Sea is insignificant. The turn point of Bohai Sea is indicated in 2013, occurring early than the East China Sea in year 2017.

https://doi.org/10.5194/egusphere-2025-4558
Preprint. Discussion started: 13 October 2025

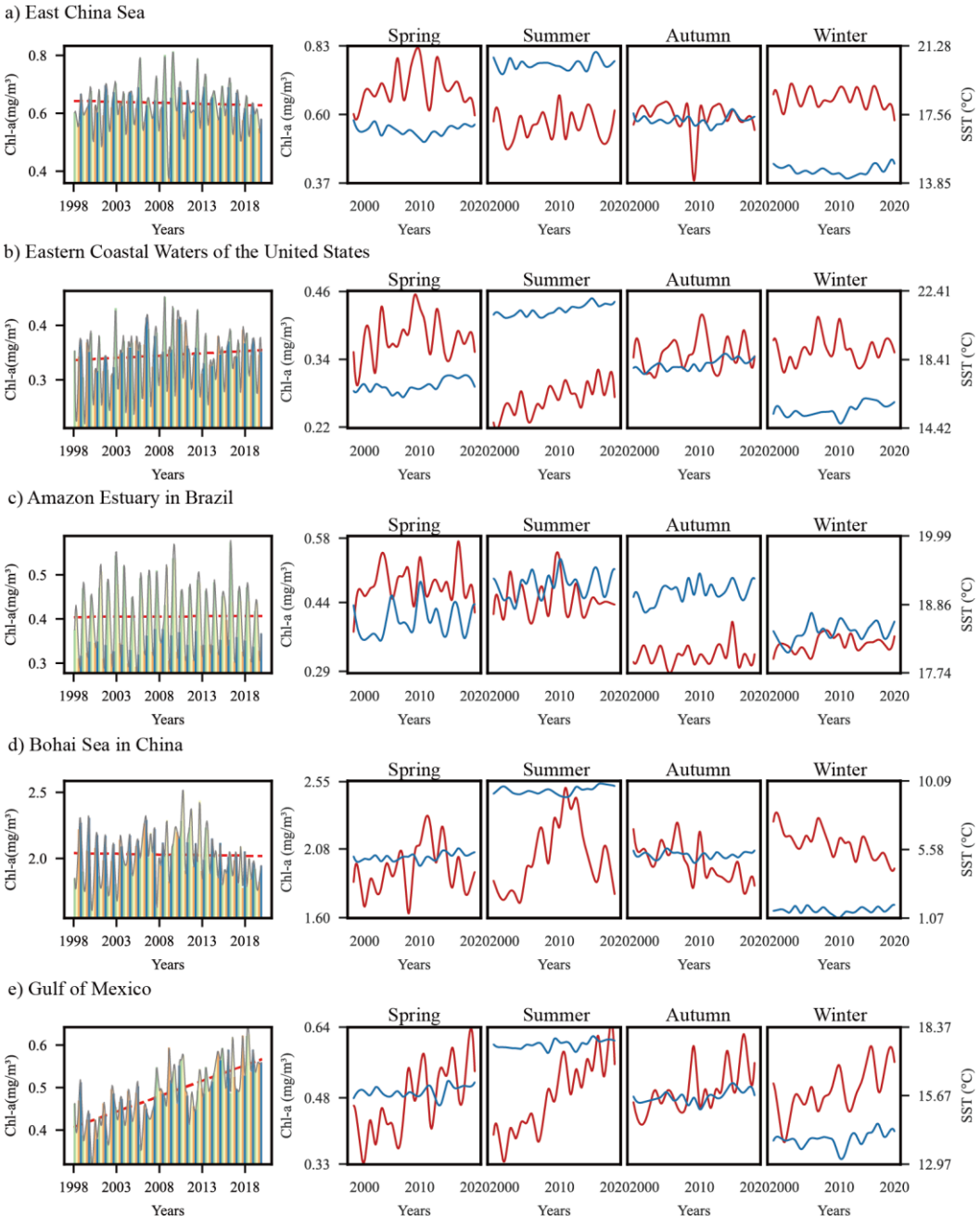

Figure 5. Historical Chl-a annual and seasonal variation for the five study locations from 1998 to 2020. The red dash line in the fisrt column represents regressive trend line. The red and blue curve line in the right four columns represent the variation of seasonal Chl-a and SST respectively.

285 The seasonal Chl-a do not always change consistently with the annual value, except in the Gulf of Mexico as shown in Fig.5. The correlation analysis between annual and seasonal Chl-a (Tab.5) suggested that the temporal change of annual Chl-a in the

https://doi.org/10.5194/egusphere-2025-4558
Preprint. Discussion started: 13 October 2025

enclosed sea areas are controlled dominantly by the spring and summer Chl-a, whereas in the open sea areas, the Chl-a in winter substitute with the summer Chl-a and becomes the second decisive factor. The Amazon Estuary is an exception, Chl-a in summer is important in determine the annual Chl-a although Chl-a in winter shows stronger correlation with the annual Chl-a.

Table 5. Correlation analysis between seasonal and annual Chl-a Concentration

Open Sea Area			Enclosed Sea Area		
Sea Area	Season	Correlation coefficient	Sea Area	Season	Correlation coefficient
East China Sea	spring	0.638	Bohai Sea	spring	0.844
	summer	0.454		summer	0.780
	fall	0.382		fall	0.284
	winter	0.496		winter	0.427
U.S. Eastern Coast	spring	0.711	Gulf of Mexico	spring	0.949
	summer	0.576		summer	0.926
	fall	0.543		fall	0.651
	winter	0.618		winter	0.905
Amazon Estuary	spring	0.735			
	summer	0.699			
	fall	0.215			
	winter	0.637			

3.3 Spatio-temporal variation of Chl-a

Fig. 6 illustrates the temporal variation rate of Chl-a concentration at each location between 1998 and 2020.The average annual and seasonal change rate of Chl-a for each of the five sea areas are shown in Appendix E. Overall, the areas with increased Chl-a are mainly located in the coastal regions, while the offshore areas in the five locations all show decreasing trends to differing degrees, with the exception of the Bohai Sea (Fig 6d).

The Bohai Sea shows the largest area with positive annual Chl-a growth rate, accounting for 33.79%, whereas the smallest area of annual growth rate of only 6.53% is observed in the waters from U.S. Eastern Coast. The most expansive area with growing seasonal Chl-a is observed in Bohai Sea in summer (Fig. 6d), while in contrast, Eastern Coastal Waters of the US had the smallest area of growing Chl-a rate in summer (Fig.6b), with only 8.06%.

https://doi.org/10.5194/egusphere-2025-4558
Preprint. Discussion started: 13 October 2025

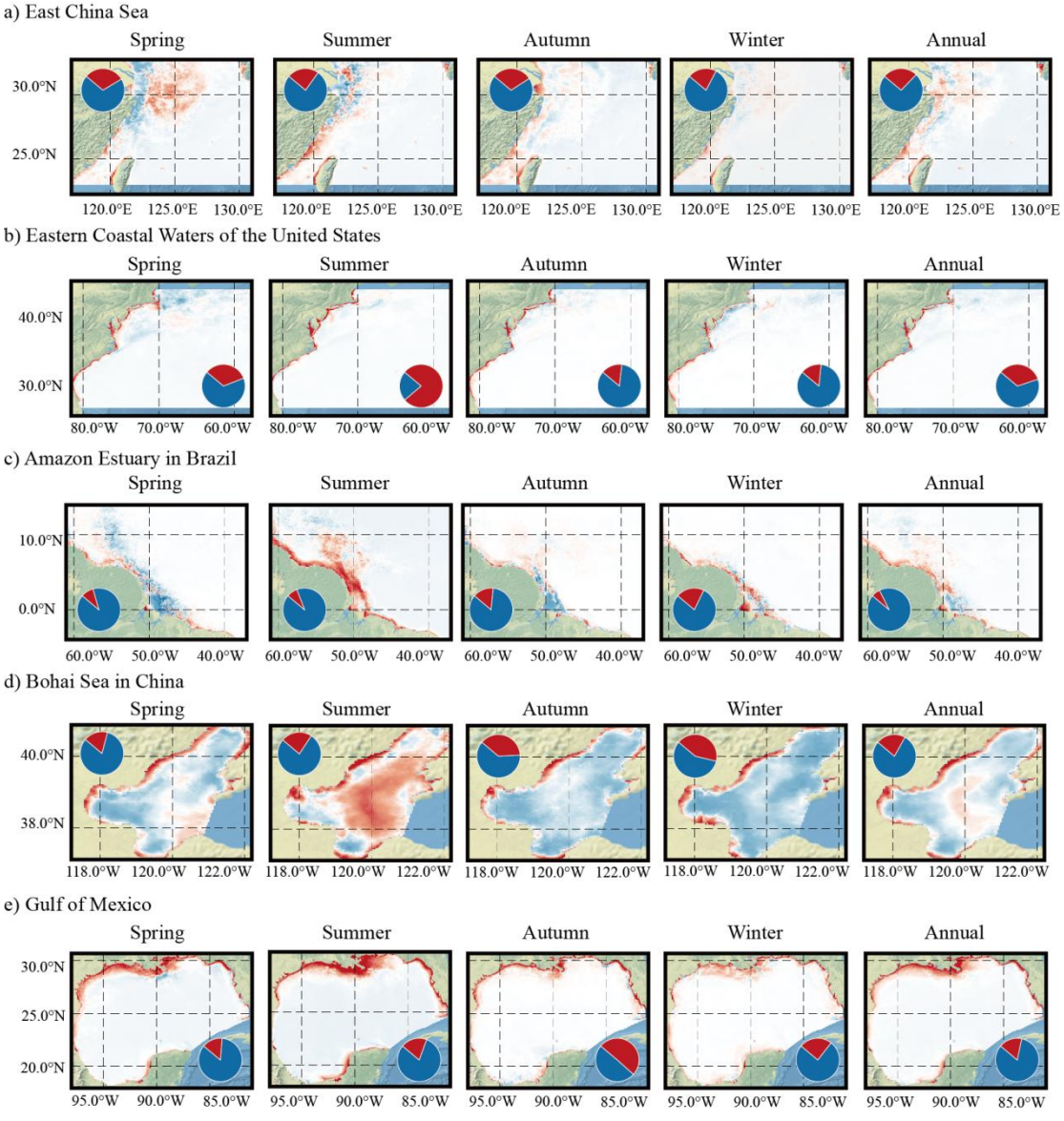

Figure 6. Temporal variation trend of Chl-a in each pixel in the five locations. a) is the average of Chl-a in spring, b is the average of Chl-a in summer, c is the average of Chl-a in autumn, d is the average of Chl-a in winter, and e is the annual average of Chl-a. The pie chart shows the proportion of areas with downward (blue) and upward (red) tendency. Areas shown in slight grey blue have no available data.

However, as illustrated in Figure 5d and 6d, a general decrease in Chl-a levels is revealed across most time frames in the context of the Bohai Sea except in the central basin of the Bohai Sea in summer, where Chl-a concentrations have exhibited a consistent upward trajectory. This anomaly is likely the ecological lag effect of nutrient aggregation in the central basin, facilitated by the internal hydrodynamical patterns and weak exchange capability with outer oceanic currents. Such nutrient

https://doi.org/10.5194/egusphere-2025-4558
Preprint. Discussion started: 13 October 2025

enrichment in the central basin, especially under the conditions of elevated summer temperatures, serves as a catalyst for algal bloom proliferation, even though the land input nutrients are undergoing anthropogenic reduction.

This dynamic, however, is intricately linked to the specific dimensions of the closed sea area and the intensity of human activities within. In contrast, the Gulf of Mexico, an analogous enclosed marine ecosystem, does not exhibit comparable patterns in fluctuations of Chl-a concentrations. This discrepancy is primarily due to the effects exerted by the Mexican Gulf Stream and the Cuban Current. These currents significantly augment the hydrological connectivity between the Gulf of Mexico and the Atlantic Ocean, thereby facilitating more vigorous exchanges of water masses. Consequently, the Chl-a concentration patterns in the Gulf of Mexico more closely resemble those observed in open sea area. In open sea areas, manifesting ascending trends in Chl-a concentrations are primarily located adjacent to coastlines and at the confluences of significant rivers and their tributaries. This is exemplified by the Changjiang estuary, as illustrated in Fig. 6a Spring, and the Amazon plume region in the summer, as evidenced in Fig. 6c.

3.4 Stability of Chl-a

The stability of Chl-a (the variation coefficient of Chl-a from 1998 to 2020) in the five locations was calculated and listed in Appendix F. Generally, regions with an obvious increasing or decreasing trend of Chl-a show low Chl-a stability, and open seas show lower stability than the enclosed seas (shown in Fig. 7), and the East China Sea shows the lowest Chl-a stability. Particularly, East China Sea, Eastern Coastal Waters of US, Amazon Estuary of Brazil and Gulf of Mexico all show instability in spring and summer, except Bohai Sea, which shows relatively high (although seasonally varying, e.g. in summer) stability. In the open ocean, significant different seasonal Chl-a stability are more pronounced (as shown in Fig. 7 a,b,c). Winter shows higher Chl-a stability in all seas. Chl-a shows lower stability of Chl-a are observed in areas like the Taiwan Strait (Fig. 7a), the Gulf Stream (Fig. 7b), and the Amazon Plume (Fig. 7c). However, Chl-a stability is higher year-round in parts of the Changjiang River (Fig. 7a) estuary and a small area near the Amazon River mouth (Fig. 7c).

The two enclosed seas show distinct Chl-a stability patterns. Particularly, the Bohai Sea has higher stability, with medium to high levels year-round, except in coastal waters and estuaries (Fig. 7d). Conversely, the Gulf of Mexico shows marked instability, with over 90% of the region having low or medium - low stability. Areas with intense human activities like the northern Gulf and Florida peninsula, show low stability year- round (Fig. 7e). Seasonal stability improves slightly in central Gulf of Mexico during winter, attributed to reduced human impacts and cooler temperatures(Durán-García et al., 2017). It is then deduced that Chl-a stability correlates with local hydrodynamic factors and anthropogenic inputs whatever in open sea area or in enclosed seas

https://doi.org/10.5194/egusphere-2025-4558
Preprint. Discussion started: 13 October 2025

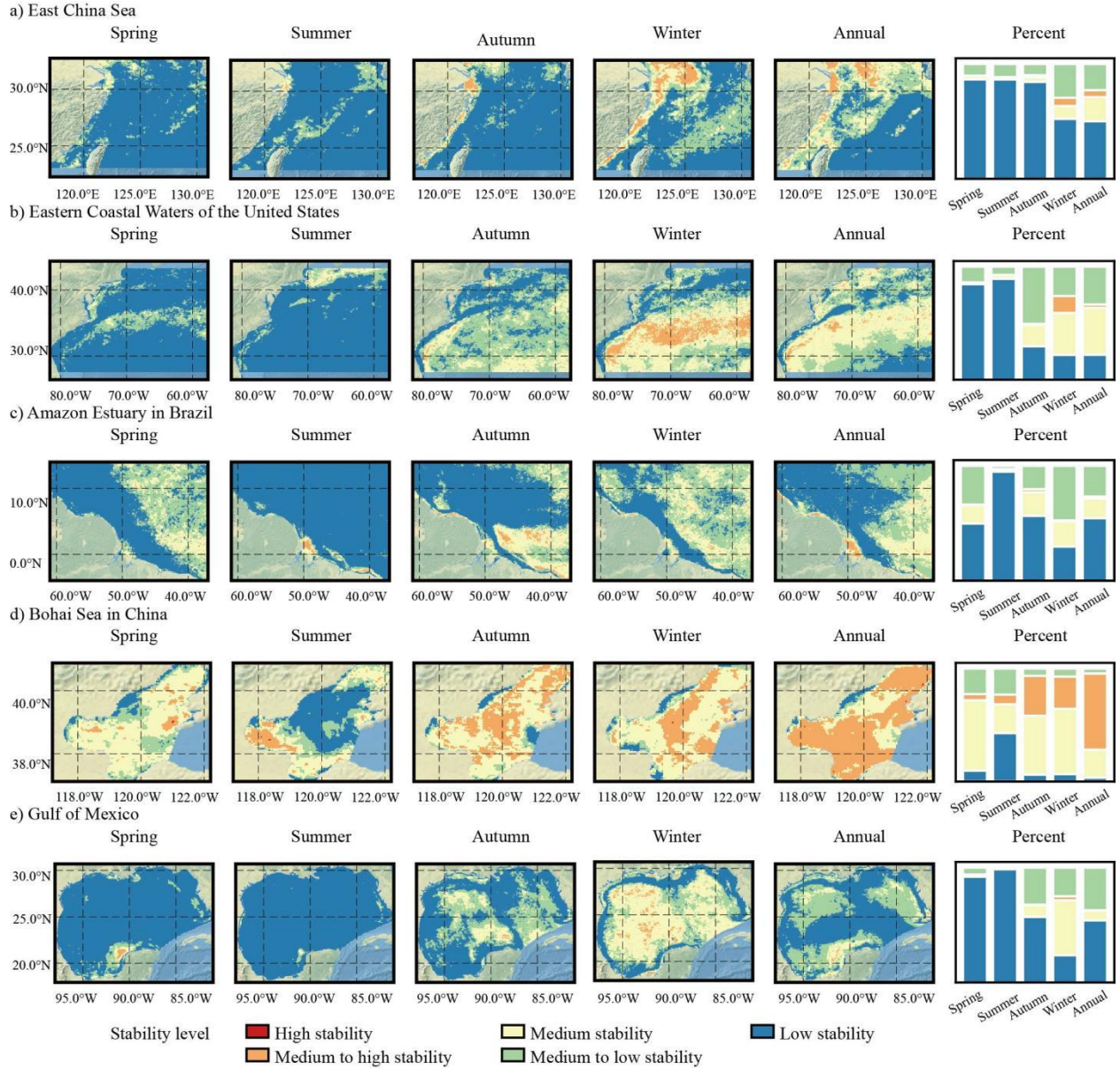

340

Figure 7. The spatial distribution of the variation coefficient of Chl-a from 1998 to 2020. A is the average of Chl-a in spring, b is the average of Chl-a in summer, c is the average of Chl-a in autumn, d is the average of Chl-a in winter, and e is the annual average of Chl-a. The percentage bar chart shows the proportion of areas with different stability in each season.

https://doi.org/10.5194/egusphere-2025-4558
Preprint. Discussion started: 13 October 2025

4 Discussion

4.1 Factors impacting spatiotemporal changes in Chl-a

To identify major environmental factors impacting the observed spatiotemporal changes in Chl-a in the five different locations, the three main environmental indices SST, PAR and SWS were correlated and evaluated with Chl-a via Pearson correlation analysis and principal component analysis, details see section 2.3.4. The correlations between Chl-a and the various marine environmental indices vary significantly depending on study area as presented in Fig. 8. In comparison with the much stronger correlation between Chl-a with SST in the East China Sea and Eastern Coastal Water of the US, and between Chl-a with PAR in Amazon Estuary, there are no obvious correlations between Chl-a and environmental indices in the two enclosed seas. In addition, no distinct correlation between Chl-a and SWS is observed in all the five locations.

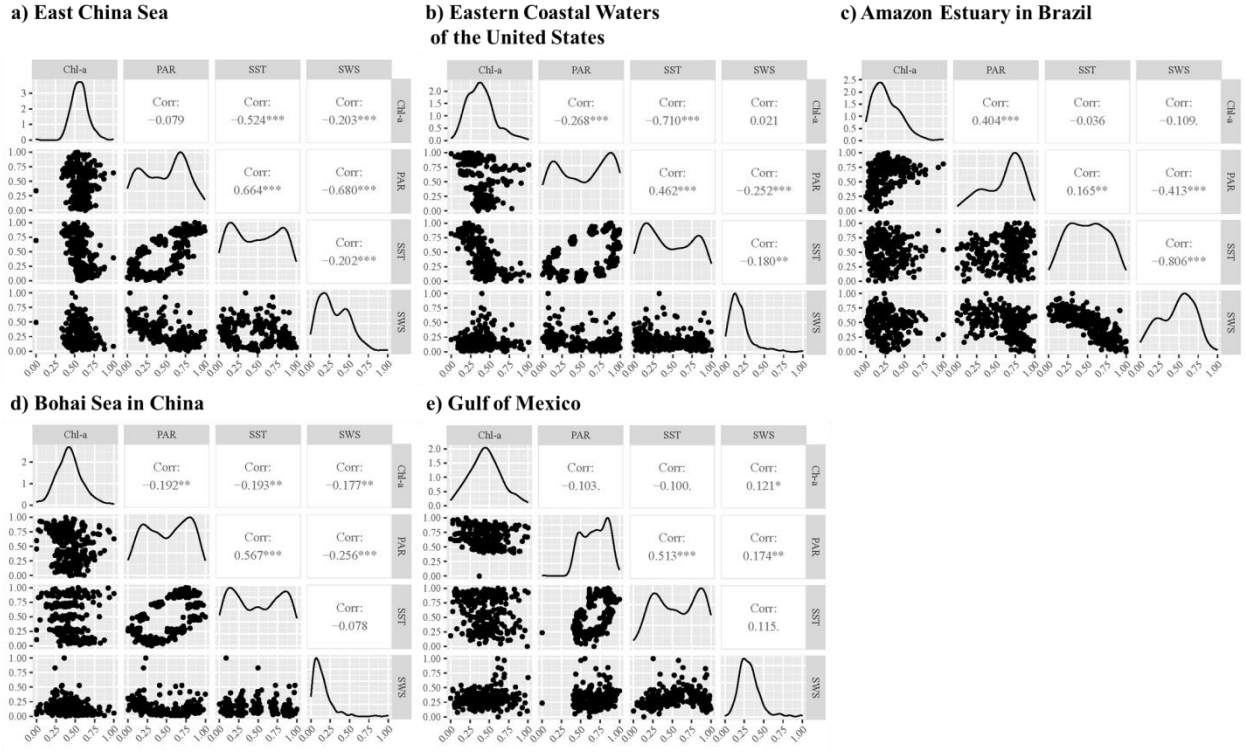

Figure 8. Spatial correlation matrices of Chl-a with environmental factors (SST, PAR, SWS) across five marginal sea areas: Color-coded data density in scatter plots (darker colours indicate higher data density), correlation coefficients (r) with significance levels ($p < 0.05$, *$p < 0.01$, $p < 0.001$) labelled, and distribution histograms for each variable

However, trends and degrees of correlations between Chl-a with SST, PAR, and SWS vary across the three open sea areas. All the three open seas show negative correlations between Chl-a and SST. Specifically, Amazon Estuary demonstrates a weaker negative correlation between Chl-a and SST than East China Sea and Eastern Coastal Waters of US, but exhibits a

https://doi.org/10.5194/egusphere-2025-4558
Preprint. Discussion started: 13 October 2025

significant positive correlation between Chl-a and PAR. A stronger negative correlation between Chl-a and SWS is observed in the East China Sea, while both Eastern Coastal Waters of US and Amazon Estuary of Brazil exhibit insignificant correlations. The weak correlation between Chl-a and SST, SWS and PAR in both the Gulf of Mexico and Bohai Sea indicate a relatively weak influence from environment on Chl-a in the enclosed sea areas.

Notably, varying degrees of inter correlations among the three indices are indicated in the five sea areas. Distinct positive correlation between SST and PAR are indicated except in Amazon Estuary. Besides, various degree of negative correlation between PAR and SWS are indicated with correlation coefficient of East China Sea >Amazon Estuary >East Coast U.S. ≈Bohai Sea, whereas Gulf of Mexico demonstrate weak positive correlation. As for the correlation between SST and SWS, strong negative correlation is only observed in Amazon Estuary, while the other four sea areas exhibit weak negative/negative correlation.

To clarify the key factors influencing on Chl-a concentration, this study conducted PCA,The results (see Table 6) indicate that SST has its largest loading (0.22 or greater) on the first principal component in all five sea areas. PAR has equal loading with SST on the first principle component in the East China Sea, while the Eastern Coastal Waters of US shows higher loading of PAR than SST on the first principle component, however, a slightly lower loading of PAR than SST is observed in Bohai Sea, and much lower than SST in Gulf of Mexico and Amazon Estuary of Brazil.

The internal correlations among the three indices indicated that seasonal SST variation in the East China Sea, Eastern Coastal Waters of US and Bohai Sea is likely to be associated more closely with seasonal PAR variation, however, due to the longer and sustained sunlight for its geographical location at the Equator with high direct solar angle, SST in the Amazon Estuary may be more susceptible to the intrusion of oceanic water rather than to the PAR. SST variation in the Gulf of Mexico is strongly related to the Gulf Stream, explaining the lower loading of PAR in the first principal component at this site. SWS has a larger load on the first principle component in the three open sea areas than in the Bohai Sea and Gulf of Mexico, which may be related to additional nutrient input from deeper sea water mixed in by the surface wind (i.e. via wind-driven water column mixing), stimulating the algal proliferation locally.

In general, the loading on the first principle component likely relates to seasonal variation of SST, PAR and SWS. The enclosed sea area of Bohai Sea and Gulf of Mexico are more susceptible to impact from seasonal SST variation, and have less impact from SWS. For the open sea areas of Eastern Coastal Waters of US and East China Sea, both the seasonal variation of SST and PAR are more important in enhancing phytoplankton biomass. In contrast, for Amazon Estuary of Brazil, which is located at the equator, the guarantee of solar irradiance makes SST independent from PAR, and PAR is less significantly impacting Chl-a than SST and SWS.

Table 6. PCA analysis for the five study locations, for the three environment indices

Sea area	Influencing factors	Principle Component 1	Principle Component 2
East China Sea	PAR	0.26	0.079

https://doi.org/10.5194/egusphere-2025-4558
Preprint. Discussion started: 13 October 2025

	SST	0.26	0.139
	SWS	0.111	0.141
Eastern Coastal Waters of US	PAR	0.29	0.147
	SST	0.245	0.175
	SWS	0.042	0.011
Amazon Estuary of Brazil	PAR	0.135	0.202
	SST	0.22	0.103
	SWS	0.208	0.022
Bohai Sea	PAR	0.234	0.146
	SST	0.286	0.123
	SWS	0.023	0.038
Gulf of Mexico	PAR	0.108	0.078
	SST	0.276	0.04
	SWS	0.024	0.113

4.2 Key factors impacting Chl-a concentration

4.2.1 Natural environmental factors

Our study revealed that SST, PAR, and SWS are critical natural indices in determining Chl-a concentration in both open and closed seas. Among them, SST has extensive impact on Chl-a levels in the study seas, depending on the time and location, especially those SST variations driven by diverse mechanisms. For example, the distinct negative correlations between SST and Chl-a in East China Sea and East Coast, U.S. indicate the inhibition of Chl-a by SST increase induced by the global warming. In this context, the influence exerted by seasonally varying SST is likely to be masked.

However, Amazon Estuary is an exception with insignificant negative correlation between Chl-a and SST. The variation of SST of the Amazon Estuary may be related more with input of low salinity Amazon plume, which creates a near surface barrier layer that inhibits mixing, increases SST, and prevents vertical mixing between the upper warm mixed layer and the cold deep ocean (Ferry and Reverdin, 2004; Balaguru et al., 2012; Grodsky et al., 2012; Coles et al.,2013). On the contrary, PAR show notable positive correlation with Chl-a in Amazon Estuary, indicating its importance in stimulating the growth of algal regionally rather than SST. PAR intensity in the Amazon Estuary is relatively steadly high although there is seasonal variation due to atmospheric circulation and precipitation patterns. however, similar to SST, the effect of PAR on Chl-a is also diverse. High turbidity may act to reduce the solar radiation available to phytoplankton and lead to regionally low biomass, such as in Hangzhou Bay, the northern Changjiang Estuary of East China Sea.

https://doi.org/10.5194/egusphere-2025-4558
Preprint. Discussion started: 13 October 2025

Open sea areas experience heightened susceptibility to SWS compared to the enclosed seas. SWS is closely related to current and upwelling activity, which have profound impacts on the Chl-a concentration particularly in the offshore regions of the three open sea areas. Several ocean circulation-influenced regions exhibit poor stability in terms of their Chl-a concentration due to upwelling of deeper seawater with suitable SST, salinity and nutrients for phytoplankton growth (as shown in Fig. 6 and Fig. 7). Moreover, the exchange with open sea water in the Bohai Sea and Gulf of Mexico also impact the Chl-a concentration, inducing relatively lower Chl-a locally as shown in Fig. 6 and Fig.7.

Different from the open seas, the two enclosed seas show very weak correlations between Chl-a and SST, PAR, SWS, which may indicate that long term change of natural environment such as SST, PAR and SWS have insignificant impact on the phytoplankton. However, the stability of the regions where large ocean currents interact with seawater (such as the sea area near the Bohai Strait and in the Gulf Stream active area) is consistently low throughout the year, suggesting the influences from the exchange of different currents. It is notable that oceanic currents is an important factor that can not be ignored, and it is closely intertwined with marine environmental indices. Besides, enclosed sea areas present a more complex seasonal pattern of Chl-a distribution. In the Bohai Sea, high Chl-a concentrations are found in coastal waters with significant seasonal shifts; spring expansion is prominent, with a peak in late summer and lowest average values due to zooplankton predation (Ministry of Water Resources, PRC, 2021; Duan et al., 2020).

4.2.2 Global warming

To exclude the impacts of seasonal variations in Chl-a and of seasonal upwelling of cooler deeper water on SST, pearson tests between SST and Chl-a during the identified global warming periods and SST stable periods as comparison at the five locations are shown in Fig. 9. It is noted that the relationship between Chl-a and SST during global warming in both open and enclosed sea areas is complex and influenced by at least two main factors, including saline water intrusion and estuarine plume effects. The general positive Chl-a-SST correlations in nearshore areas may be stimulated by the huge land nutrients input accompanied with seawater temperature rising, while the predominant negative correlations in offshore regions, especially during SST rise can be closely related with heating oligotrophic saline seawater intrusion.

https://doi.org/10.5194/egusphere-2025-4558
Preprint. Discussion started: 13 October 2025

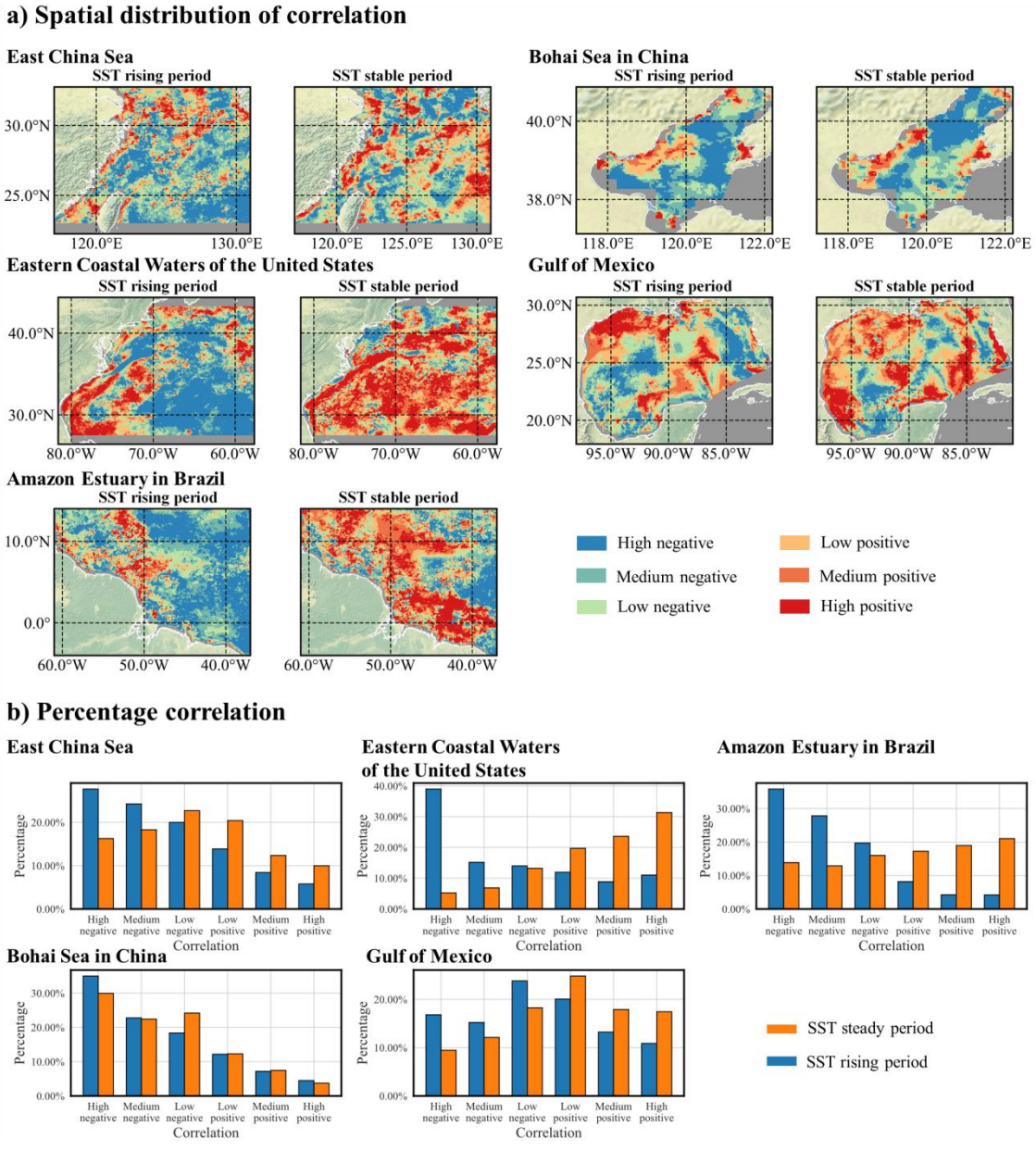

Figure 9. Spatial distribution and percentage correlation of SST change with Chl-a in five marginal sea areas (1998-2020): (a) Spatial distribution of Pearson correlation coefficients during SST rising periods (high SST change rate) and SST stable periods (low SST change rate), with color key: blue = high negative correlation (Chl-a decreases with SST rise), green = medium negative correlation, orange = medium positive correlation, red = high positive correlation (Chl-a increases with SST rise), light green = low negative correlation; (b) Percentage distribution of correlation strengths in different sea areas during SST rising (blue bars) and stable periods (orange bars), showing the proportion of high/medium/low negative and positive correlations.

In open sea areas like the East China Sea and East Coast of the US, Chl-a-SST correlations vary distinctly during rising and stable SST periods. Compared to the enclosed sea areas, the open sea areas are more significantly affected by temperature variations, the proportion of correlations during rising and stable SST periods exhibits an almost completely opposite

https://doi.org/10.5194/egusphere-2025-4558
Preprint. Discussion started: 13 October 2025

distribution pattern. During SST rise, the area with negative correlations increases significantly in East China Sea, reaching 71.92% of the total, and similarly in Eastern Coastal Waters of US at 68.15%. The stronger negative correlations during SST rise, mainly distributed in the areas with the saline intrusion. Notably, nearshore areas and estuarine plume-influenced regions like the Changjiang River estuary (Fig. 9a East China sea) consistently show positive Chl-a-SST correlations regardless of temperature changes.

In enclosed sea areas like the Bohai Sea and the Gulf of Mexico, Chl-a-SST correlations also display significant negative correlations during SST rise. For example, in Bohai Sea, the negative correlation area reaches 76.14%, with spatial variability. Areas with positive correlations are mainly in specific regions like Liaodong Bay and the Luanhe River mouth. In Gulf of Mexico, the negative correlation area constitutes 55.85% of the total sea area, more pronounced in coastal regions like Tampa and the west central Gulf (Fig. 9a Gulf of Mexico). This pattern may be estuarine plume influence, providing nutrients and enhancing Chl-a in some areas despite the overall negative correlation trend. Enclosed sea areas consistently show stronger negative Chl-a-SST correlations during SST rise than stable periods, suggesting temperature increases detrimentally affect phytoplankton biomass in these regions.

4.2.3 Anthropogenic nutrient inputs

Nutrient input is indicated to be the main anthropogenic factor stimulating extensive Chl-a increases in the five study locations, particularly in the estuaries and the nearshore areas along the coast, regardless of whether they are enclosed or open sea areas. Moreover, the environmental impacts of nutrients released by human activities may be further amplified by active upwelling currents and other ocean currents in the coastal and estuarine zones. In the East China Sea, high Chl-a concentrations are primarily associated with the Changjiang Estuary and the presence of the TWC, exhibiting significant seasonal variation (Dai et al., 2022; Shi et al., 2023). Spring sees a surge in Chl-a due to nutrient-rich runoff from the Changjiang River, with a subsequent decline through summer and autumn, and a moderate increase in winter influenced by the CRP and the TWC. Similarly, the East Coast of the United States demonstrates a gradient of decreasing Chl-a from nearshore to offshore and northwest to southeast, with seasonal peaks in spring and winter (Fig 4f), attributed to coastal bay nutrient dynamics. The Amazon Estuary also reflects seasonal variability, with spring and summer high Chl-a areas expanding northeastward (Fig 4c), driven by nutrient inflows from the Amazon River.

Certain regions in Bohai Sea, such as Laizhou Bay and the Liao River Estuary sustain high Chl-a throughout the year, likely due to strong anthropogenic nutirents input under weaker hydrodynamic forces. In contrast, the Gulf of Mexico showcases high Chl-a zones around the Mississippi River estuary and the Campeche Bay, where anthropogenic discharges and coastal upwelling play substantial roles (Martínez-López and Zavala-Hidalgo, 2009). Autumn sees a notable decrease in the Mississippi estuary Chl-a, coinciding with the river's lowest runoff period, while the central Gulf of Mexico maintains stable low Chl-a levels.

Regionally, eastern China has been experiencing rapid industrial development and urbanization with increasing population density since the 1980s. Bohai Sea and East China Sea are adjacent to the Bohai Economic Rim and “the economic zone of

https://doi.org/10.5194/egusphere-2025-4558
Preprint. Discussion started: 13 October 2025

Changjiang River Delta" of eastern China respectively. These two sea areas receive huge anthropogenic nutrient inputs which drives an overall increase in Chl-a during the study period. The Chl-a concentration in both the Bohai Sea and East China Sea exceed that of the Gulf of Mexico, Eastern Coastal Waters of US, and Amazon Estuary of Brazil(Röthig et al., 2023). However, Gulf of Mexico shows the highest rate of Chl-a increase, which may be related to intensifying human activities. For other regions, It should be noted that fertilizer use by Brazil is increasing and is second behind China (https://ourworldindata.org/fertilizers), which may greatly increase nutrients in the Amazon Estuary also. Chl-a in the Bohai Sea has however exhibited a declining trend since 4 and a decreasing rate of Chl-a concentration increase in the East China Sea has been observed from 2017 as well, which may be a result of a reduction of pollutant emission due to strict implementation of environmental control policies by the Chinese government.

Chl-a concentrations in the central basin of the Bohai Sea show a continued increase over time and remain relatively high. In addition, the outer Changjiang estuary (under the impact of the plume of Changjiang Diluted Water) shows significant increase in Chl-a, even though there is an obvious Chl-a decrease in the inner Changjiang Estuary (a similar phenomenon is observed in the plume of the Amazon Estuary of Brazil, especially in the summer (Fig. 6)). This indicates that the long-term influence of land-sourced nutrient inputs is still expanding to more offshore regions. The effect of human activities on phytoplankton biomass trends far surpasses other (natural) effects in the estuaries, bay and nearshore areas of the Bohai Sea and the East China Sea, including any negative impacts of SST rise and increased thermal stratification on nutrient supply.

5 Conclusions

In this study, a Chl-a time series dataset spanning 1998 to 2020 was created using monthly products from SeaWiFS/Chl-a and MODIS/Chl-a L3 products. The spatial and temporal variability of Chl-a in the Bohai Sea and Gulf of Mexico, East China Sea, Eastern Coastal Waters of US and Amazon Estuary of Brazil was examined in relation to various degrees of anthropogenic disturbance and global warming, taking into account factors such as SWS, PAR, and other controls. The following conclusions were drawn from this research:

5.1 The double edge of SST on Chl-a

This study demonstrates two main impacts on Chl-a concentration from rising SST. Generally, the widespread areas which show positive correlations between SST and Chl-a during stable SST periods (as shown in Fig. 9a Gulf of Mexico and Fig.9a Amazon Estuary of Brazil) are indicated to be related to seasonal SST variation. Additional anthropogenic nutrient inputs combined with the rising SST may stimulate phytoplankton proliferation, leading to increasing Chl-a along the coast in all five sea areas studied. Despite the control of pollutant emissions to the Bohai Sea and East China Sea, a continuous increase in Chl-a in the central Bohai Sea and the plume area of the Changjiang Diluted Water in East China Sea are observed, although there is reduced Chl-a along coasts and estuaries as shown in Fig. 6 East China Sea Annual and Fig. 6 Bohai Sea Annual.

https://doi.org/10.5194/egusphere-2025-4558
Preprint. Discussion started: 13 October 2025

Meanwhile, a significant inhibitory effect of SST rise on Chl-a during typical warming periods is indicated. Negative correlations between Chl-a and SST are observed in most offshore areas which is consistent with saline sea water intrusion and influence of large current systems, such as the TWC in the East China Sea, Gulf Stream along Eastern Coastal Waters of US, and the North Brazilian Current in Amazon Estuary of Brazil. However, negative impacts from rising SST on nutrient supply are concealed by (land-derived) nutrient induced Chl-a enhancement especially in nearshore areas, and in the plumes of estuaries in the East China Sea and Amazon Estuary of Brazil. It is important to note that in the Amazon Estuary of Brazil, despite a significant increase of Chl-a in nearshore areas in 2020 compared to 2018, the overall Chl-a concentrations show a decreasing trend. This means that the falling trend in Chl-a in the offshore region owing to global warming effects may no longer be compensated for by additional anthropogenic nutrient inputs combining with rising SST in the coastal region and the estuary.

For the enclosed sea areas, the Gulf of Mexico exhibits a much lower level of eutrophication compared to the Bohai Sea. With larger spatial area, the connectivity between Gulf of Mexico and the Atlantic Ocean is enhanced by the presence of the Gulf Stream and the Cuban Current, leading to more frequent exchange of water masses. Consequently, the impact of seawater warming on the Gulf of Mexico is more pronounced than on the Bohai Sea. Therefore, the environmental conditions in the Gulf of Mexico more resemble those of the open sea, and a significant decrease in Chl-a concentration is observed during periods of SST increase in the Gulf of Mexico, as shown in Fig. 9a Gulf of Mexico.

5.2 Chl-a variation tendency under global warming and human response

The impact of global warming on Chl-a concentration is evident in all three open sea areas, namely the Amazon Estuary of Brazil, East China Sea and Eastern Coastal Waters of US. Significant decreases in offshore Chl-a levels, attributed to global warming rather than human activity, have been observed. If SSTs continue to rise and the contribution of riverine nutrients inputs decreases due to long-term pollution control measures, this ecological effect may extend to nearshore areas. Additionally, in the enclosed sea area of the Gulf of Mexico with medium eutrophic characteristics, the negative influence of global warming on Chl-a has also been identified. Rising SSTs and oceanic currents have led to a noticeable decline in Chl-a, particularly in areas where ocean currents enter the Gulf of Mexico. The negative correlation between SST and Chl-a in the central Gulf further supports the detrimental impact of global warming on Chl-a levels.

However, the impacts of rising SSTs under global warming in estuaries and along coastal waters are less pervasive than those from eutrophication. Eutrophication-induced phytoplankton blooms are expanding into offshore sea areas, even though Chl-a levels may decline along the coast due to controls on anthropogenic nutrient inputs. In highly eutrophic confined sea areas, such as the Bohai Sea, Chl-a levels appear to be less impacted by rising SSTs under global warming. Despite a decline in Chl-a concentrations in coastal waters of the Bohai Sea, the central basin still maintains high levels of Chl-a due to anthropogenic nutrient inputs, which masks the potential impact of global warming.

In the highly eutrophic open sea of the East China Sea, although there has been a significant decline in the rate of Chl-a increase in estuaries and along the coast, Chl-a levels in the plume of the Changjiang Diluted Water continue to rise. This suggests that

https://doi.org/10.5194/egusphere-2025-4558
Preprint. Discussion started: 13 October 2025

in sea areas with sufficient nutrients and suitable salinity, rising SST may further stimulate algal blooms. A similar phenomenon has been observed in the plume of the Amazon Estuary of Brazil, where the area of high Chl-a has expanded. Despite the widespread occurrence of decreasing Chl-a offshore, the continuous proliferation of phytoplankton in the plume compensates for the intrusion of warmer and oligotrophic pelagic waters.

This study contributes to our understanding of the ecological response of marine environments to both human activity and global warming. By continuously controlling the input of land-sourced nutrients, the frequency of algal blooms can be reduced, but high Chl-a levels may persist in estuaries and along the coast over the long term. From a broader perspective, nearshore areas will gradually experience greater impacts from global warming on nutrient supply. The study: (a) demonstrates the complex (and spatially variable) interactions between primary production, SST, and nutrient inputs and exchange under the dual pressures of changes in human activity and coastal development, and global warming; and (b) highlights the need for further research on the impacts of changing coastal and fluvial nutrient inputs (including where these have been reduced due to environmental protection measures) on primary productivity in both enclosed and open sea areas.

Author Contributions

X.Z. conceived the study and acquired funding and project administration and resource and supervision; N.Y. and X.Z. managed the data and method; N.Y. and S.M. performed the investigation and developed the software and validation; N.Y. and X.Z. analyzed the data; N.Y. ,X.Z. and A.C. visualized the results and wrote the original draft; and L.B., A.C., H.J., and R.L. reviewed and edited the manuscript.

Acknowledgments

This study was funded by Zhejiang Provincial Natural Science Foundation of China under Grant No. LD24D060001, and National Natural Science Foundation of China (U22B2012).

Open Research

The code for data processing, analysis, and plotting in this study is available on GitHub at the following URL: https://github.com/giseryn/Chlorophyll-a-Variation-Trends-in-Marginal-Seas. Additionally, the data used in the paper can be downloaded online, Chl-a data and photosynthetically active radiation data is available from NASA (https://oceancolor.gsfc.nasa.gov/l3/order/).Sea surface temperature data is available from NOAA (https://www.ncei.noaa.gov/products/avhrr-pathfinder-sst). the ocean polygon data is available from Natural Earth (https://www.naturalearthdata.com/). The Basin population density data was made utilizing the LandScan (2020) High Resolution Global Population Data Set.

https://doi.org/10.5194/egusphere-2025-4558
Preprint. Discussion started: 13 October 2025

References

Baker, K. G. and Geider, R. J.: Phytoplankton mortality in a changing thermal seascape, Global Change Biology, 27, 5253–5261, https://doi.org/10.1111/gcb.15772, 2021.

Behrenfeld, M. J., O'Malley, R. T., Boss, E. S., Westberry, T. K., Graff, J. R., Halsey, K. H., Milligan, A. J., Siegel, D. A., and Brown, M. B.: Revaluating ocean warming impacts on global phytoplankton, Nature Clim Change, 6, 323–330, https://doi.org/10.1038/nclimate2838, 2016.

Boyce, D. G., Lewis, M. R., and Worm, B.: Global phytoplankton decline over the past century, Nature, 466, 591–596, https://doi.org/10.1038/nature09268, 2010a.

Boyce, D. G., Lewis, M. R., and Worm, B.: Global phytoplankton decline over the past century, Nature, 466, 591–596, https://doi.org/10.1038/nature09268, 2010b.

Cai, W., Santoso, A., Collins, M., Dewitte, B., Karamperidou, C., Kug, J.-S., Lengaigne, M., McPhaden, M. J., Stuecker, M. F., Taschetto, A. S., Timmermann, A., Wu, L., Yeh, S.-W., Wang, G., Ng, B., Jia, F., Yang, Y., Ying, J., Zheng, X.-T., Bayr, T., Brown, J. R., Capotondi, A., Cobb, K. M., Gan, B., Geng, T., Ham, Y.-G., Jin, F.-F., Jo, H.-S., Li, X., Lin, X., McGregor, S., Park, J.-H., Stein, K., Yang, K., Zhang, L., and Zhong, W.: Changing El Niño–Southern Oscillation in a warming climate, Nat Rev Earth Environ, 2, 628–644, https://doi.org/10.1038/s43017-021-00199-z, 2021.

Cai, W., Ng, B., Wang, G., Santoso, A., Wu, L., and Yang, K.: Increased ENSO sea surface temperature variability under four IPCC emission scenarios, Nat. Clim. Chang., 12, 228–231, https://doi.org/10.1038/s41558-022-01282-z, 2022.

Campos-Silva, J. V., Peres, C. A., Amaral, J. H. F., Sarmento, H., Forsberg, B., and Fonseca, C. R.: Fisheries management influences phytoplankton biomass of Amazonian floodplain lakes, Journal of Applied Ecology, 58, 731–743, https://doi.org/10.1111/1365-2664.13763, 2021.

Chen, C.-C., Shiah, F.-K., Gong, G.-C., and Chen, T.-Y.: Impact of upwelling on phytoplankton blooms and hypoxia along the Chinese coast in the East China Sea, Marine Pollution Bulletin, 167, 112288, https://doi.org/10.1016/j.marpolbul.2021.112288, 2021.

Chowdhury, K. M. A., Jiang, W., Liu, G., Ahmed, Md. K., and Akhter, S.: Dominant physical-biogeochemical drivers for the seasonal variations in the surface chlorophyll-a and subsurface chlorophyll-a maximum in the Bay of Bengal, Regional Studies in Marine Science, 48, 102022, https://doi.org/10.1016/j.rsma.2021.102022, 2021.

Cui, D., Liang, S., and Wang, D.: Observed and projected changes in global climate zones based on Köppen climate classification, WIREs Climate Change, 12, e701, https://doi.org/10.1002/wcc.701, 2021.

Dai, M., Su, J., Zhao, Y., Hofmann, E. E., Cao, Z., Cai, W.-J., Gan, J., Lacroix, F., Laruelle, G. G., Meng, F., Müller, J. D., Regnier, P. A. G., Wang, G., and Wang, Z.: Carbon Fluxes in the Coastal Ocean: Synthesis, Boundary Processes, and Future Trends, Annu. Rev. Earth Planet. Sci., 50, 593–626, https://doi.org/10.1146/annurev-earth-032320-090746, 2022.

Dai, Y., Yang, S., Zhao, D., Hu, C., Xu, W., Anderson, D. M., Li, Y., Song, X.-P., Boyce, D. G., Gibson, L., Zheng, C., and Feng, L.: Coastal phytoplankton blooms expand and intensify in the 21st century, Nature, 615, 280–284, https://doi.org/10.1038/s41586-023-05760-y, 2023.

Damien, P., Sheinbaum, J., Pasqueron de Fommervault, O., Jouanno, J., Linacre, L., and Duteil, O.: Do Loop Current eddies stimulate productivity in the Gulf of Mexico?, Biogeosciences, 18, 4281–4303, https://doi.org/10.5194/bg-18-4281-2021, 2021.

https://doi.org/10.5194/egusphere-2025-4558
Preprint. Discussion started: 13 October 2025

Dobson, J. E., Bright, E. A., Coleman, P. R., Durfee, R. C., and Worley, B. A.: LandScan: a global population database for estimating populations at risk, Photogrammetric engineering and remote sensing, 66, 849–857, 2000.

Duan, H., Wang, C., Liu, Z., Wang, H., Wu, X., and Xu, J.: Summer wind gusts modulate transport through a narrow strait, Bohai, China, Estuarine, Coastal and Shelf Science, 233, 106526, https://doi.org/10.1016/j.ecss.2019.106526, 2020.

Durán-García, R., Méndez-González, M., and Larqué-Saavedra, A.: The Biodiversity of the Yucatan Peninsula: A Natural Laboratory, in: Progress in Botany Vol. 78, edited by: Cánovas, F. M., Lüttge, U., and Matyssek, R., Springer International Publishing, Cham, 237–258, https://doi.org/10.1007/124_2016_8, 2017.

Favareto, L., Brotas, V., Rudorff, N., Zacarias, N., Tracana, A., Lamas, L., Nascimento, Â., Ferreira, A., Gomes, M., Borges, C., Palma, C., and Brito, A. C.: Response of phytoplankton to coastal upwelling: The importance of temporal and spatial scales, Limnology and Oceanography, 68, 1376–1387, https://doi.org/10.1002/lno.12353, 2023.

Field, C. B., Behrenfeld, M. J., Randerson, J. T., and Falkowski, P.: Primary production of the biosphere: integrating terrestrial and oceanic components, Science, 281, 237–240, https://doi.org/10.1126/science.281.5374.237, 1998.

Frau, D., Gutierrez, M. F., Molina, F. R., and de Mello, F. T.: Drivers assessment of zooplankton grazing on phytoplankton under different scenarios of fish predation and turbidity in an in situ mesocosm experiment, Hydrobiologia, 848, 485–498, https://doi.org/10.1007/s10750-020-04456-y, 2021.

Friedlingstein, P., O'Sullivan, M., Jones, M. W., Andrew, R. M., Gregor, L., Hauck, J., Le Quéré, C., Luijkx, I. T., Olsen, A., Peters, G. P., Peters, W., Pongratz, J., Schwingshackl, C., Sitch, S., Canadell, J. G., Ciais, P., Jackson, R. B., Alin, S. R., Alkama, R., Arneth, A., Arora, V. K., Bates, N. R., Becker, M., Bellouin, N., Bittig, H. C., Bopp, L., Chevallier, F., Chini, L. P., Cronin, M., Evans, W., Falk, S., Feely, R. A., Gasser, T., Gehlen, M., Gkritzalis, T., Gloege, L., Grassi, G., Gruber, N., Gürses, Ö., Harris, I., Hefner, M., Houghton, R. A., Hurtt, G. C., Iida, Y., Ilyina, T., Jain, A. K., Jersild, A., Kadono, K., Kato, E., Kennedy, D., Klein Goldewijk, K., Knauer, J., Korsbakken, J. I., Landschützer, P., Lefèvre, N., Lindsay, K., Liu, J., Liu, Z., Marland, G., Mayot, N., McGrath, M. J., Metzl, N., Monacci, N. M., Munro, D. R., Nakaoka, S.-I., Niwa, Y., O'Brien, K., Ono, T., Palmer, P. I., Pan, N., Pierrot, D., Pocock, K., Poulter, B., Resplandy, L., Robertson, E., Rödenbeck, C., Rodriguez, C., Rosan, T. M., Schwinger, J., Séférian, R., Shutler, J. D., Skjelvan, I., Steinhoff, T., Sun, Q., Sutton, A. J., Sweeney, C., Takao, S., Tanhua, T., Tans, P. P., Tian, X., Tian, H., Tilbrook, B., Tsujino, H., Tubiello, F., van der Werf, G. R., Walker, A. P., Wanninkhof, R., Whitehead, C., Willstrand Wranne, A., et al.: Global Carbon Budget 2022, Earth System Science Data, 14, 4811–4900, https://doi.org/10.5194/essd-14-4811-2022, 2022.

Fu, Z., Hu, L., Chen, Z., Zhang, F., Shi, Z., Hu, B., Du, Z., and Liu, R.: Estimating spatial and temporal variation in ocean surface pCO2 in the Gulf of Mexico using remote sensing and machine learning techniques, Science of The Total Environment, 745, 140965, https://doi.org/10.1016/j.scitotenv.2020.140965, 2020.

Geng, T., Cai, W., Jia, F., and Wu, L.: Decreased ENSO post-2100 in response to formation of a permanent El Niño-like state under greenhouse warming, Nat Commun, 15, 5810, https://doi.org/10.1038/s41467-024-50156-9, 2024.

Gregg, W. W. and Rousseaux, C. S.: Decadal trends in global pelagic ocean chlorophyll: A new assessment integrating multiple satellites, in situ data, and models, Journal of Geophysical Research: Oceans, 119, 5921–5933, https://doi.org/10.1002/2014JC010158, 2014.

Gregg, W. W., Casey, N. W., and McClain, C. R.: Recent trends in global ocean chlorophyll, Geophysical Research Letters, 32, https://doi.org/10.1029/2004GL021808, 2005.

Hallegraeff, G. M., Anderson, D. M., Belin, C., Bottein, M.-Y. D., Bresnan, E., Chinain, M., Enevoldsen, H., Iwataki, M., Karlson, B., McKenzie, C. H., Sunesen, I., Pitcher, G. C., Provoost, P., Richardson, A., Schweibold, L., Tester, P. A., Trainer,

https://doi.org/10.5194/egusphere-2025-4558
Preprint. Discussion started: 13 October 2025

V. L., Yñiguez, A. T., and Zingone, A.: Perceived global increase in algal blooms is attributable to intensified monitoring and emerging bloom impacts, Commun Earth Environ, 2, 1–10, https://doi.org/10.1038/s43247-021-00178-8, 2021.

Hong, Z., Long, D., Li, X., Wang, Y., Zhang, J., Hamouda, M. A., and Mohamed, M. M.: A global daily gap-filled chlorophyll-*a* dataset in open oceans during 2001–2021 from multisource information using convolutional neural networks, Earth System Science Data, 15, 5281–5300, https://doi.org/10.5194/essd-15-5281-2023, 2023.

Hou, Z., Li, J., Diao, Y., Zhang, Y., Zhong, Q., Feng, J., and Qi, X.: Asymmetric influences of ENSO phases on the predictability of North Pacific sea surface temperature, Geophysical Research Letters, 51, e2023GL108091, 2024.

IPCC: Climate Change 2021: The Physical Science Basis. Contribution of Working Group I to the Sixth Assessment Report of the Intergovernmental Panel on Climate Change, Cambridge University Press, Cambridge, United Kingdom and New York, NY, USA, https://doi.org/10.1017/9781009157896, 2021.

Jickells, T. D.: Nutrient Biogeochemistry of the Coastal Zone, Science, 281, 217–222, https://doi.org/10.1126/science.281.5374.217, 1998.

Jin, D., Hoagland, P., and Buesseler, K. O.: The value of scientific research on the ocean's biological carbon pump, Science of The Total Environment, 749, 141357, https://doi.org/10.1016/j.scitotenv.2020.141357, 2020.

Ju, X., Ma, C., Yao, Z., and Bao, X.: Case analysis of water exchange between the Bohai and Yellow Seas in response to high winds in winter, J. Ocean. Limnol., 38, 30–41, https://doi.org/10.1007/s00343-019-9100-2, 2020.

Kaiser, J., Abel, S., Arz, H. W., Cundy, A. B., Dellwig, O., Gaca, P., Gerdts, G., Hajdas, I., Labrenz, M., Milton, J. A., Moros, M., Primpke, S., Roberts, S. L., Rose, N. L., Turner, S. D., Voss, M., and Ivar do Sul, J. A.: The East Gotland Basin (Baltic Sea) as a candidate Global boundary Stratotype Section and Point for the Anthropocene series, The Anthropocene Review, 10, 25–48, https://doi.org/10.1177/20530196221132709, 2023.

Kong, C. E., Yoo, S., and Jang, C. J.: East China Sea ecosystem under multiple stressors: Heterogeneous responses in the sea surface chlorophyll-a, Deep Sea Research Part I: Oceanographic Research Papers, 151, 103078, https://doi.org/10.1016/j.dsr.2019.103078, 2019.

Lebakula, V., Sims, K., Reith, A., Rose, A., McKee, J., Coleman, P., Kaufman, J., Urban, M., Jochem, C., Whitlock, C., Ogden, M., Pyle, J., Roddy, D., Epting, J., and Bright, E.: LandScan Global 30 Arcsecond Annual Global Gridded Population Datasets from 2000 to 2022, Sci Data, 12, 495, https://doi.org/10.1038/s41597-025-04817-z, 2025.

Lee, K. H., Jeong, H. J., Lee, K., Franks, P. J. S., Seong, K. A., Lee, S. Y., Lee, M. J., Hyeon Jang, S., Potvin, E., Suk Lim, A., Yoon, E. Y., Yoo, Y. D., Kang, N. S., and Kim, K. Y.: Effects of warming and eutrophication on coastal phytoplankton production, Harmful Algae, 81, 106–118, https://doi.org/10.1016/j.hal.2018.11.017, 2019.

Letscher, R. T., Moore, J. K., Martiny, A. C., and Lomas, M. W.: Pico-phytoplankton contribute half of global marine carbon export, https://doi.org/10.22541/essoar.167768119.97557585/v1, 2023.

Lloyd, C. T., Chamberlain, H., Kerr, D., Yetman, G., Pistolesi, L., Stevens, F. R., Gaughan, A. E., Nieves, J. J., Hornby, G., MacManus, K., Sinha, P., Bondarenko, M., Sorichetta, A., and Tatem, A. J.: Global spatio-temporally harmonised datasets for producing high-resolution gridded population distribution datasets, Big Earth Data, 3, 108–139, https://doi.org/10.1080/20964471.2019.1625151, 2019.

Ma, J. and Smith, W. O. J.: Primary Productivity in the Mid-Atlantic Bight: Is the Shelf Break a Location of Enhanced Productivity?, Front. Mar. Sci., 9, https://doi.org/10.3389/fmars.2022.824303, 2022.

https://doi.org/10.5194/egusphere-2025-4558
Preprint. Discussion started: 13 October 2025

Maćkiewicz, A. and Ratajczak, W.: Principal components analysis (PCA), Computers & Geosciences, 19, 303–342, https://doi.org/10.1016/0098-3004(93)90090-R, 1993.

Mao, Z., Gu, X., Cao, Y., Zhang, M., Zeng, Q., Chen, H., Shen, R., and Jeppesen, E.: The Role of Top-Down and Bottom-Up Control for Phytoplankton in a Subtropical Shallow Eutrophic Lake: Evidence Based on Long-Term Monitoring and Modeling, Ecosystems, 23, 1449–1463, https://doi.org/10.1007/s10021-020-00480-0, 2020.

Marrari, M., Piola, A. R., Valla, D., and Wilding, J. G.: Trends and variability in extended ocean color time series in the main reproductive area of the Argentine hake, Merluccius hubbsi (Southwestern Atlantic Ocean), Remote Sensing of Environment, 177, 1–12, https://doi.org/10.1016/j.rse.2016.02.011, 2016.

Martinez, E., Gorgues, T., Lengaigne, M., Fontana, C., Sauzède, R., Menkes, C., Uitz, J., Di Lorenzo, E., and Fablet, R.: Reconstructing Global Chlorophyll-a Variations Using a Non-linear Statistical Approach, Frontiers in Marine Science, 7, 2020.

Martínez-López, B. and Zavala-Hidalgo, J.: Seasonal and interannual variability of cross-shelf transports of chlorophyll in the Gulf of Mexico, Journal of Marine Systems, 77, 1–20, https://doi.org/10.1016/j.jmarsys.2008.10.002, 2009.

Mears, C. A., Scott, J., Wentz, F. J., Ricciardulli, L., Leidner, S. M., Hoffman, R., and Atlas, R.: A Near-Real-Time Version of the Cross-Calibrated Multiplatform (CCMP) Ocean Surface Wind Velocity Data Set, Journal of Geophysical Research: Oceans, 124, 6997–7010, https://doi.org/10.1029/2019JC015367, 2019.

Ministry of Ecology and Environment, PRC: China marine environmental quality bulletin, 2001.

Ministry of Ecology and Environment, PRC: Bulletin of Marine Ecology and Environment Status of China in 2020, 2021.

Ministry of Water Resources, PRC: Bulletin of Chinese river sediment (2020) The Ministry of Water Resources of the People's Republic of China, 2021.

Mizuta, D. D. and Wikfors, G. H.: Can offshore HABs hinder the development of offshore mussel aquaculture in the northeast United States?, Ocean & Coastal Management, 183, 105022, https://doi.org/10.1016/j.ocecoaman.2019.105022, 2020.

Moradi, M. and Moradi, N.: Correlation between concentrations of chlorophyll-a and satellite derived climatic factors in the Persian Gulf, Marine Pollution Bulletin, 161, 111728, https://doi.org/10.1016/j.marpolbul.2020.111728, 2020.

Mudelsee, M.: Trend analysis of climate time series: A review of methods, Earth-Science Reviews, 190, 310–322, https://doi.org/10.1016/j.earscirev.2018.12.005, 2019.

Pi, X., Zhao, S., Wang, W., Liu, D., Xu, C., Han, G., Kuang, T., Sui, S.-F., and Shen, J.-R.: The pigment-protein network of a diatom photosystem II–light-harvesting antenna supercomplex, Science, 365, eaax4406, 2019.

Pisano, A., Buongiorno Nardelli, B., Tronconi, C., and Santoleri, R.: The new Mediterranean optimally interpolated pathfinder AVHRR SST Dataset (1982–2012), Remote Sensing of Environment, 176, 107–116, https://doi.org/10.1016/j.rse.2016.01.019, 2016.

Reid, P. C., Battle, E. J. V., Batten, S. D., and Brander, K. M.: Impacts of fisheries on plankton community structure, ICES Journal of Marine Science, 57, 495–502, https://doi.org/10.1006/jmsc.2000.0740, 2000.

Röthig, T., Trevathan-Tackett, S. M., Voolstra, C. R., Ross, C., Chaffron, S., Durack, P. J., Warmuth, L. M., and Sweet, M.: Human-induced salinity changes impact marine organisms and ecosystems, Global Change Biology, 29, 4731–4749, https://doi.org/10.1111/gcb.16859, 2023.

https://doi.org/10.5194/egusphere-2025-4558
Preprint. Discussion started: 13 October 2025

Shi, Y., Zhang, M., Xu, X., He, M., Liu, Y., Du, J., Zhao, M., Wei, Q., Liu, D., and Gao, J.: Ecological effects of offshore transport in the shelf sea and its response to climate warming, Global and Planetary Change, 229, 104240, https://doi.org/10.1016/j.gloplacha.2023.104240, 2023.

Siemer, J. P., Machín, F., González-Vega, A., Arrieta, J. M., Gutiérrez-Guerra, M. A., Pérez-Hernández, M. D., Vélez-Belchí, P., Hernández-Guerra, A., and Fraile-Nuez, E.: Recent Trends in SST, Chl-a, Productivity and Wind Stress in Upwelling and Open Ocean Areas in the Upper Eastern North Atlantic Subtropical Gyre, Journal of Geophysical Research: Oceans, 126, e2021JC017268, https://doi.org/10.1029/2021JC017268, 2021.

Subramaniam, A., Yager, P. L., Carpenter, E. J., Mahaffey, C., Björkman, K., Cooley, S., Kustka, A. B., Montoya, J. P., Sañudo-Wilhelmy, S. A., Shipe, R., and Capone, D. G.: Amazon River enhances diazotrophy and carbon sequestration in the tropical North Atlantic Ocean, Proceedings of the National Academy of Sciences, 105, 10460–10465, https://doi.org/10.1073/pnas.0710279105, 2008.

Wang, H., Fu, D., Liu, D., Xiao, X., He, X., and Liu, B.: Analysis and Prediction of Significant Wave Height in the Beibu Gulf, South China Sea, Journal of Geophysical Research: Oceans, 126, e2020JC017144, https://doi.org/10.1029/2020JC017144, 2021.

Wang, X.: Advance in the Inter-annual Variability of Vegetation and Its Relation to Climate Based on Remote Sensing, Journal of remote sensing, 421–431, https://doi.org/10.11834/jrs.20060363, 2006.

Wang, Y. and Xiu, P.: Typhoon footprints on ocean surface temperature and chlorophyll-*a* in the South China Sea, Science of The Total Environment, 840, 156686, https://doi.org/10.1016/j.scitotenv.2022.156686, 2022.

Xi, H., Losa, S. N., Mangin, A., Garnesson, P., Bretagnon, M., Demaria, J., Soppa, M. A., Hembise Fanton d'Andon, O., and Bracher, A.: Global Chlorophyll a Concentrations of Phytoplankton Functional Types With Detailed Uncertainty Assessment Using Multisensor Ocean Color and Sea Surface Temperature Satellite Products, Journal of Geophysical Research: Oceans, 126, e2020JC017127, https://doi.org/10.1029/2020JC017127, 2021.

Yingling, N., Kelly, T. B., Shropshire, T. A., Landry, M. R., Selph, K. E., Knapp, A. N., Kranz, S. A., and Stukel, M. R.: Taxon-specific phytoplankton growth, nutrient utilization and light limitation in the oligotrophic Gulf of Mexico, Journal of Plankton Research, 44, 656–676, https://doi.org/10.1093/plankt/fbab028, 2022.

Zhang, C., Hu, C., Shang, S., Müller-Karger, F. E., Li, Y., Dai, M., Huang, B., Ning, X., and Hong, H.: Bridging between SeaWiFS and MODIS for continuity of chlorophyll-a concentration assessments off Southeastern China, Remote Sensing of Environment, 102, 250–263, https://doi.org/10.1016/j.rse.2006.02.015, 2006.

Zhang, W., Li, S., Jin, F.-F., Xie, R., Liu, C., Stuecker, M. F., and Xue, A.: ENSO Regime Changes Responsible for Decadal Phase Relationship Variations Between ENSO Sea Surface Temperature and Warm Water Volume, Geophysical Research Letters, 46, 7546–7553, https://doi.org/10.1029/2019GL082943, 2019.

Zhou, Z.-X., Yu, R.-C., and Zhou, M.-J.: Evolution of harmful algal blooms in the East China Sea under eutrophication and warming scenarios, Water Research, 221, 118807, https://doi.org/10.1016/j.watres.2022.118807, 2022.

https://doi.org/10.5194/egusphere-2025-4558
Preprint. Discussion started: 13 October 2025

Appendix

Appendix A：Chl-a concentration and PAR fitting equations obtained from SeaWiFS and MODIS satellites for each study area

The overlapped Chl-a data from MODIS and SeaWiFS data during the T2 period were processed with linear regression equations for each month in various sea areas ($y = ax + b$, x, y are the Chl-a values of SeaWiFS and MODIS, respectively); and data with R2 below 0.5 were not corrected. When R2 was greater than 0.5, the equation derived from this linear regression was used to correct SeaWiFS\Chl-a. The regression results values for each sea area are listed in Appendix A. The construction methods are shown as follows:

T1 period: corrected SeaWiFS\Chl-a values substitute for the original data of corresponding months ($\mathrm{Chl-a_{SWFcorr}}$). For months without correction, the original SeaWiFS\Chl-a ($\mathrm{Chl-a_{SWF}}$) are used.

T2 period: Chl-a values are calculated through averaging the data from MODIS ($\mathrm{Chl-a_{MOD}}$) and SeaWiFS($\mathrm{Chl-a_{SWFcorr}}$/$\mathrm{Chl-a_{SWF}}$).

$$\mathrm{Chl-a_{T2}} = (\mathrm{Chl-a_{SWF}} + \mathrm{Chl-a_{MOD}})/2$$

$$\mathrm{Chl-a_{T2}} = (\mathrm{Chl-a_{SWFCORR}} + \mathrm{Chl-a_{MOD}})/2$$

T3 period: only MODIS\Chl-a data are available, $\mathrm{Chl-a_{MOD}}$ are used directly.

Months that require correction Chl-a concentration in the East China Sea include April, August, September, and December.

$$y = 0.661x + 0.251$$

$$y = 0.571x + 0.233$$

$$y = 0.246x + 0.400$$

$$y = 0.439x + 0.323$$

Months that require correction Chl-a concentration in the Eastern Coastal Waters of US include April, August, November.

$$y = 0.672x + 0.145$$

$$y = 0.835x + 0.086$$

$$y = 1.007x + 0.008$$

Months that require correction Chl-a concentration in the Amazon Estuary of Brazil include June, August, December.

$$y = 0.48x + 0.233$$

$$y = 0.519x + 0.198$$

$$y = 0.735x + 0.091$$

Months that require correction Chl-a concentration in the Bohai Sea include June, August, December .

$$y = 0.851x + 0.424$$

$$y = 1.052x + 0.154$$

$$y = 0.735x + 0.091$$

https://doi.org/10.5194/egusphere-2025-4558
Preprint. Discussion started: 13 October 2025

Months that require correction Chl-a concentration in the Gulf of Mexico include March, April, May, June, July, August, November, December.

$$y = 0.937x + 0.071$$
$$y = 0.902x + 0.090$$
$$y = 0.758x + 0.132$$
$$y = 0.614x + 0.192$$
$$y = -0.021x + 0.558$$
$$y = 0.366x + 0.328$$
$$y = 1.139x + 0.009$$
$$y = 1.061x + 0.033$$

Months that require correction PAR data in the East China Sea include January, February, March, April, June, August, October, November, December.

$$y = 0.7407x + 3.0500$$
$$y = 0.9062x + 1.2272$$
$$y = 0.6633x + 7.4084$$
$$y = 1.1265x \pm 4.7338$$
$$y = 0.9306x + 0.3926$$
$$y = 0.5859x + 15.0874$$
$$y = 0.5185x + 12.0817$$
$$y = 0.8109x + 2.7642$$
$$y = 0.4869x + 6.9225$$

Months that require correction PAR data in the Amazon Estuary of Brazil include January, February, March, April, May, June, August, November, December.

$$y = 0.6712x + 9.4768$$
$$y = 1.1324x \pm 4.8767$$
$$y = 1.1223x \pm 4.8357$$
$$y = 0.9561x + 1.1267$$
$$y = 0.9114x + 2.4527$$
$$y = 0.6899x + 9.6201$$
$$y = 0.8800x + 4.0144$$
$$y = 0.5721x + 12.6073$$
$$y = 1.1020x \pm 3.2767$$

Months that require correction PAR data in the Bohai Sea include January, February, March, April, June, November, December.

https://doi.org/10.5194/egusphere-2025-4558
Preprint. Discussion started: 13 October 2025

$$y = 1.1750x \pm 1.8659$$
$$y = 1.2591x \pm 3.4065$$
$$y = 0.4278x + 8.6293$$
$$y = 0.6687x + 5.9476$$
$$y = 0.9130x + 1.2173$$
$$y = 0.8262x + 1.2522$$
$$y = 0.4056x + 4.1002$$

Months that require correction PAR data in the Gulf of Mexico include January, February, March, April, June, November, December.

$$y = 1.0927x \pm 2.2949$$
$$y = 0.9091x + 2.7284$$
$$y = 1.2825x \pm 10.5483$$
$$y = 0.3289x + 21.2346$$
$$y = 1.0825x \pm 1.7048$$
$$y = 1.1187x + -2.0893$$

Appendix B: Outlier Removal in Time Series Analysis

In order to achieve reliability and stability when calculating the monthly average Chl-a concentration, it is necessary to eliminate outliers in the Daily Chl-a time series., a statistical approach based on three times the standard deviation was applied to identify and eliminate outliers. The method follows the assumption that data points lying beyond three standard deviations from the mean are statistically rare and likely to represent anomalies. Mathematically, the criteria for identifying outliers can be expressed as:

$$X_{outlier} \notin [\mu - 3\sigma, \mu + 3\sigma]$$

Where $X_{outlier}$ represents the outlier values, μ is the mean of the data, and σ is the standard deviation. Data points outside the range $[\mu - 3\sigma, \mu + 3\sigma]$ were flagged as outliers and excluded from further analysis.

This approach ensures that extreme values, which might unduly influence statistical results or model performance, are systematically removed. The method is particularly effective for time series datasets that approximate a normal distribution. For non-normally distributed data, additional validation steps were taken to ensure the robustness of this approach. The outlier elimination process was iterated as necessary to maintain consistency and accurately reflect the underlying temporal trends in the dataset.

https://doi.org/10.5194/egusphere-2025-4558
Preprint. Discussion started: 13 October 2025

Appendix C：Slope Trend Analysis

The annual variation rate slope of Chl-a from 1998 to 2020 is calculated using the least squares method. This method determines the linear trend in the data by fitting a straight line through the time series, where the slope represents the average annual rate of change. The slope is calculated using the following formula:

$$\text{Slope} = \frac{n\sum_{i=1}^{n}(i \times Chla_i) - \sum_{i=1}^{n} i \sum_{i=1}^{n} Chla_i}{n \times \sum_{i=1}^{n} i - \sum_{i=1}^{n} i}$$

This formula minimizes the residual errors between the observed Chl-a values and the values predicted by the fitted line, ensuring the most accurate representation of the trend. The slope obtained provides a quantitative measure of the rate of change in Chl-a concentration over the period. A positive slope indicates an increasing trend in Chl-a concentrations, while a negative slope signifies a decreasing trend.

Appendix D：Stability Analysis

The stability of a time series over time can be evaluated using C_v, which provides a standardized measure of the dispersion of the data relative to its mean. This is particularly useful for understanding the consistency of values in the time series across the observed period. The formula for C_v is expressed as:

$$C_v = \frac{1}{\bar{x}}\sqrt{\frac{\sum_{i=1}^{n}(x_i - \bar{x}^2)}{n-1}}$$

A lower C_v indicates greater stability in the time series, with less variation relative to the mean, while a higher C_v suggests more significant fluctuations over time.

Appendix E：Areas with increasing or decreasing trend of Chl-a from 1998 to 2020

sea area	Season	Trend	Ratio of the total area	sea area	Season	Trend	Ratio of the total area
East China Sea	Spring	Decreasing	69.74%	Bohai Sea	Spring	Decreasing	67.06%
		Increasing	30.26%			Increasing	32.94%
	Summer	Decreasing	76.24%		Summer	Decreasing	22.34%
		Increasing	23.76%			Increasing	77.66%
	Autumn	Decreasing	70.21%		Autumn	Decreasing	84.35%
		Increasing	29.79%			Increasing	15.65%
	Winter	Decreasing	78.44%		Winter	Decreasing	84.40%
		Increasing	21.56%			Increasing	15.60%

https://doi.org/10.5194/egusphere-2025-4558
Preprint. Discussion started: 13 October 2025

	annual	Decreasing	73.89%		annual	Decreasing	66.21%
		Increasing	26.11%			Increasing	33.79%
sea area	Season	Trend	Ratio of the total area	sea area	Season	Trend	Ratio of the total area
Eastern Coastal Waters of US	Spring	Decreasing	90.57%	Gulf of Mexico	Spring	Decreasing	81.97%
		Increasing	9.42%			Increasing	17.96%
	Summer	Decreasing	91.85%		Summer	Decreasing	76.81%
		Increasing	8.06%			Increasing	23.11%
	Autumn	Decreasing	84.65%		Autumn	Decreasing	61.87%
		Increasing	15.34%			Increasing	38.01%
	Winter	Decreasing	78.97%		Winter	Decreasing	57.38%
		Increasing	21.02%			Increasing	42.54%
	annual	Decreasing	93.47%		annual	Decreasing	77.97%
		Increasing	6.53%			Increasing	21.94%

sea area	Season	Trend	Ratio of the total area
Amazon Estuary of Brazil	Spring	Decreasing	84.77%
		Increasing	15.23%
	Summer	Decreasing	80.51%
		Increasing	19.49%
	Autumn	Decreasing	49.49%
		Increasing	50.51%
	Winter	Decreasing	75.56%
		Increasing	24.43%
	annual	Decreasing	82.81%
		Increasing	17.19%

https://doi.org/10.5194/egusphere-2025-4558
Preprint. Discussion started: 13 October 2025

860 **Appendix F：Annual and seasonal stability of Chl-a in the five location from 1998-2020**

		BS	GM	ECS	ECW	AE
	Level of Stability	Ratio of the Area	Ratio of the Area	Ratio of the Area	Ratio of the Area	Ratio of the Area
annual	High	0.11%	0.00%	0.01%	0.01%	0.00%
	Medium to high	67.51%	0.42%	6.13%	2.91%	1.67%
	Medium	24.62%	8.42%	21.05%	41.54%	17.13%
	Medium to low	4.28%	36.98%	22.73%	33.43%	26.77%
	Low	3.47%	54.18%	50.08%	22.11%	54.43%
spring	High	0.06%	0.00%	0.00%	0.00%	0.00%
	Medium to high	5.46%	0.47%	0.05%	0.03%	0.45%
	Medium	62.33%	1.50%	3.11%	1.61%	16.04%
	Medium to low	22.58%	6.03%	10.13%	13.86%	33.75%
	Low	9.57%	92.01%	86.71%	84.50%	49.76%
summer	High	0.06%	0.00%	0.00%	0.00%	0.01%
	Medium to high	8.61%	0.00%	0.27%	0.15%	0.76%
	Medium	25.43%	0.25%	1.90%	3.21%	1.61%
	Medium to low	23.02%	1.17%	11.32%	7.24%	2.73%
	Low	42.87%	98.59%	86.51%	89.40%	94.89%
autumn	High	0.00%	0.00%	0.00%	0.00%	0.00%
	Medium to high	35.17%	0.28%	1.73%	0.64%	2.72%
	Medium	52.14%	10.36%	4.12%	19.33%	20.54%
	Medium to low	6.50%	32.19%	9.66%	50.55%	20.27%
	Low	6.18%	57.17%	84.48%	29.47%	56.47%
winter	High	0.02%	0.00%	0.04%	0.03%	0.00%
	Medium to high	28.44%	3.59%	7.19%	14.96%	0.67%

https://doi.org/10.5194/egusphere-2025-4558
Preprint. Discussion started: 13 October 2025

Medium	57.77%	47.75%	11.15%	37.26%	22.07%
Medium to low	7.12%	24.81%	29.39%	25.90%	47.55%
Low	6.65%	23.84%	52.24%	21.84%	29.71%